

Sensing Diamagnetic Electrolytes with Spin Defects in Diamond

Fabian A. Freire-Moschovitis,[†] Roberto Rizzato,[†] Anton Pershin,[‡] Moritz R. Schepp,[†] Robin D. Allert,[†] Lina M. Todenhagen,[¶] Martin S. Brandt,[¶] Ádám Gali,^{‡,§} and Dominik B. Bucher^{*,†}

[†]*TUM School of Natural Sciences, Department of Chemistry, Technical University of Munich, Lichtenbergstraße 4, 85748 Garching bei München, Germany*

[‡]*Wigner Research Centre for Physics, Institute for Solid State Physics and Optics, PO. Box 49, Budapest H-1525, Hungary*

[¶]*Walter Schottky Institut and Physik-Department, Technical University of Munich, Am Coulombwall 4, 85748 Garching bei München, Germany*

[§]*Department of Atomic Physics, Institute of Physics, Budapest University of Technology and Economics, Műegyetem rakpart 3, Budapest H-1111, Hungary*

E-mail: dominik.bucher@tum.de

Abstract

Quantum sensing with spin defects in diamond, such as the nitrogen vacancy (NV) center, enables the detection of various chemical species on the nanoscale. Molecules or ions with unpaired electronic spins are typically probed by their influence on the NV-center's spin relaxation. Whereas it is well-known that paramagnetic ions reduce the NV-center's relaxation time (T_1), here we report on the opposite effect for diamagnetic ions. We demonstrate that millimolar concentrations of aqueous diamagnetic electrolyte solutions increase the T_1 time of near-surface NV-center ensembles compared

to pure water. To elucidate the underlying mechanism of this surprising effect, single and double quantum NV experiments are performed, which indicate a reduction of magnetic and electric noise in the presence of diamagnetic electrolytes. In combination with *ab initio* simulations, we propose that a change in the interfacial band bending due to the formation of an electric double layer leads to a stabilization of fluctuating charges at the interface of an oxygen-terminated diamond. This work not only helps to understand noise sources in quantum systems but also broadens the application space of quantum sensors towards electrolyte sensing in cell biology, neuroscience and electrochemistry.

Introduction

Nitrogen vacancy (NV) centers in diamond offer a broad platform for quantum sensing applications ranging from the measurement of basic physical properties, such as temperature,¹ pressure,² strain,³ electric⁴ and magnetic fields^{5,6} down to single cells,⁷ single molecules,⁸ or even single nuclear spins.^{9,10} This unprecedented sensitivity is achieved due to the atomic size of the qubit enabling its location only a few nanometer away from the diamond interface (see Figure 1a).¹¹ Near surface NV-centers (≤ 20 nm below the surface) can be used to sense nuclear magnetic resonance (NMR)^{8,12–15} and electron spin resonance (ESR) signals¹⁶ from nanoscale chemical and biological samples. The NV-center translates these magnetic field fluctuations directly to an optical signal, detected by a change in the fluorescence intensity. Together with optical spin state initialization with green laser light and coherent spin state manipulation with microwave pulses, these key features make the NV-center a unique tool for (bio)chemical analysis.^{11,15,17,18}

NV-centers are also perceptive to electric fields.^{4,19} Even a single elementary charge located ~ 150 nm away from the quantum sensor produces a strong enough static electric field to affect an NV-center's ODMR (optically detected magnetic resonance) transitions.⁴ This high sensitivity of NV-centers to magnetic or electric fields marks a narrow ridge: On the

one hand, it allows for single nuclear spin or elementary charge detection, on the other hand it makes the qubit prone to magnetic or electronic spin noise in its close environment. This is particularly relevant for NV-centers close to the surface, where interfacial processes and defects cause additional noise and reduce the performance of the NV-quantum sensors.^{20–23}

Due to the NV-center’s susceptibility to a broad range of frequencies (from DC to GHz),²⁴ noise can be measured by applying different sensing protocols.¹⁸ High frequency noise (\sim GHz) can be probed by the longitudinal spin-lattice relaxation time (T_1) with a protocol that is usually referred to as NV-relaxometry.^{17,18,24–26} The T_1 time defines the time constant of the spin-state-dependent fluorescence decay from the magnetic sublevel $m_s = 0$ (bright state) to thermal equilibrium (mixed state) and is on the order of a few milliseconds for near-surface NV-ensembles in bulk diamonds,¹¹ or on the order of a few hundred microseconds for nanodiamonds (depending on their size).¹⁷ Generally, any magnetic noise overlapping with the NV-center’s Larmor frequency (on the order of the zero-field splitting $D = 2.87$ GHz) will decrease the T_1 relaxation time (see Figure 1b).^{18,25,27,28} Relaxometry has been successfully applied to map high frequency magnetic noise originating from inside the diamond (e.g. paramagnetic impurities²⁹), at the diamond interface (e.g. dangling bonds^{20,30}) or from samples on top of the diamond (e.g. organic radicals^{27,31} or paramagnetic ions, such as Mn^{2+} ,³² Fe^{3+} ,³³ or Gd^{3+} ^{25,28}). Furthermore, nanoscale NV-relaxometry has also been used to determine the pH value³⁴ or to monitor chemical reactions *in situ*.³⁵

While the increase of the relaxation rate due to paramagnetic species has been studied extensively, herein we detect the opposite effect for diamagnetic ions. When near-surface NV-centers in oxygen-terminated diamonds are exposed to aqueous diamagnetic electrolytes, we observe a systematic extension of the T_1 relaxation time compared to pure (deionized) water. We show that this unexpected effect is proportional to the electrolyte concentration, reversible and dependent on the NV-center’s implantation depth. In order to shed light on the underlying sensing mechanism, we perform single and double quantum relaxometry experiments which indicate a reduction of electric as well as magnetic noise. Furthermore,

double electron electron resonance (DEER) spectroscopy experiments show a similar effect on surface dark spins, which possibly act as surface reporter spins. In combination with theoretical methods including *ab initio* simulations of the diamond/electrolyte interface, we propose that diamagnetic ions alter the interfacial band bending. This leads to a stabilization of fluctuating charges at the interface and to the increase of the T_1 relaxation time.

Results

T_1 Relaxometry on Electrolytes with Near-Surface NV-Center Ensembles

In this study we use near-surface high dense NV-center ensembles (implanted with ^{15}N at an energy of 2.5 keV and a fluence of $2 \times 10^{12} \text{ cm}^{-2}$), distributed $\sim 5 \text{ nm}$ underneath the diamond surface,^{13,36,37} to investigate the effect of aqueous electrolyte solutions on the spin-lattice relaxation time T_1 probed by NV-relaxometry. Before experiments are conducted, we prepare the diamond surface with a tri-acid clean procedure according to Brown *et al.*³⁸ This procedure not only ensures to remove non-diamond carbon material from the interface but also creates an oxygen-terminated surface comprised of mixed carbon oxide species including hydroxyl groups, ethers, ketones, aldehydes and carboxylic acids.³⁹ We position the diamond in a microfluidic device that guarantees controllable in- and output of the applied liquids, prevents sample evaporation and provides a constant and defined volume for following measurements (see Figure 1a).¹⁵ Importantly, the microfluidic device avoids a direct contact between the liquid and the microwave delivery.

The NV-relaxometry protocol is depicted in Figure 1b and essentially consists of two 532 nm laser pulses of 5 μs duration for optical spin state initialization and readout separated by a sweep time t . A subsequent measurement with a $\pi_{0,-1}$ -pulse (where the subscripts 0 and -1 indicate transitions between $m_s = 0 \leftrightarrow m_s = -1$) at the start is used for normalization and noise cancellation purposes.¹⁸ The T_1 time can be extracted from the (bi)exponential fit of

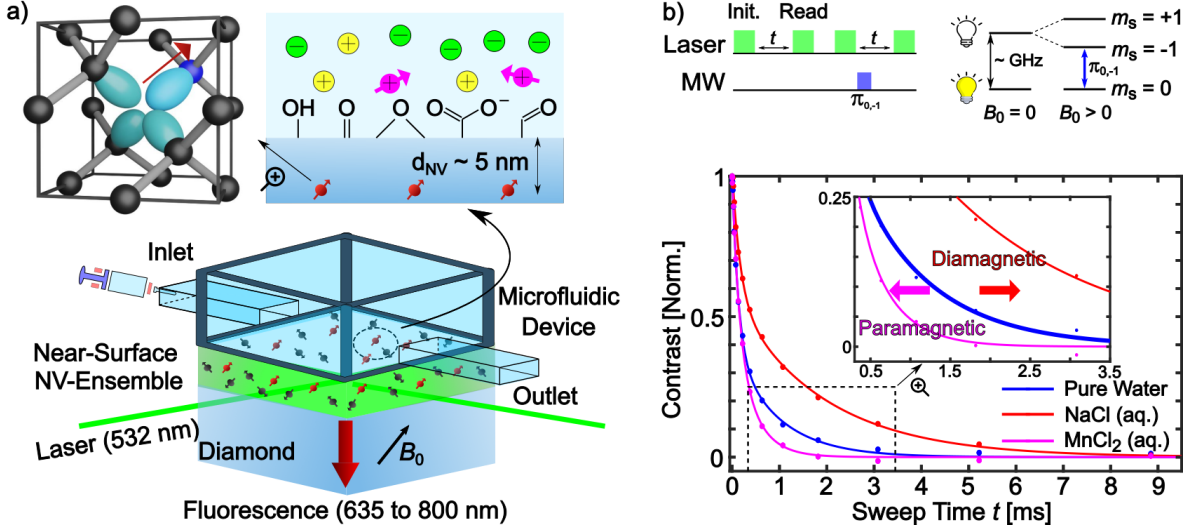


Figure 1: **Scheme of NV-relaxometry experiments with aqueous electrolyte solutions.** a) Top (left): The NV-center in the diamond crystal lattice. A nitrogen atom (blue) replaces a carbon atom (black) in the crystal. Together with an adjacent vacancy an NV-center is formed. The orbitals (petrol) indicate four possible NV-center orientations within the diamond lattice. Top (right): Scheme of an oxygen-terminated diamond surface with an ensemble of near-surface NV-centers ($d_{NV} \sim 5$ nm). The oxygen termination consists of hydroxyl groups, ethers, ketones, aldehydes and carboxylic acids. We probe pure water, paramagnetic (purple) and diamagnetic (yellow) ions. Bottom: A microfluidic device placed on top of the diamond. In- and outlet allow for adding and removing aqueous electrolyte solutions or pure water from the diamond surface. b) Top (left): NV-relaxometry pulse sequence. Two laser pulses for spin state initialization and read-out are separated by a sweep time (t). A consecutive measurement with a π -pulse at the start is used for noise cancellation.¹⁸ Top (right): Energy levels of the NV-center's electronic ground state ($S = 1$). The zero-field splitting ($D = 2.87$ GHz) separates the $m_s = 0$ (bright) and $m_s = \pm 1$ states (dark). A bias magnetic field B_0 splits the degenerate $m_s = \pm 1$ states according to the Zeeman effect. Bottom: T_1 relaxation curves of pure water and solutions of NaCl (500 mM) and MnCl₂ (1 μ M). While paramagnetic MnCl₂ reduces the T_1 relaxation time with respect to pure water, diamagnetic NaCl extends the relaxation time. Experiments are performed at $f_{NV} = 1.88$ GHz.

the relaxation curves depicting the contrast as a function of sweep time t (see Supplementary Note 1 for fitting details).

We perform the measurements by filling the microfluidic channel and covering the diamond surface either with pure water or aqueous electrolyte solutions (see Methods for detail). Figure 1b depicts the T_1 relaxation curves when water and solutions of diamagnetic NaCl or paramagnetic MnCl_2 cover the diamond surface. Paramagnetic MnCl_2 (1 μM) on the diamond leads to a T_1 time reduction of 0.47 ± 0.19 with respect to water, which is in accordance with other studies and can be ascribed to the strong dipole-dipole interaction of the NV-center with the paramagnetic species.^{25,32} In contrast, when we repeat the same experiment with diamagnetic NaCl (500 mM) solution, we observe an extension of the T_1 time by a factor of 2.04 ± 0.45 compared to water. Experiments supporting this observation are also conducted with other diamagnetic salt solutions (mono-, di- and trivalent) and reveal similar results (see Supplementary Note 2). Therefore, we choose NaCl as a representative of a standard diamagnetic electrolyte for the following measurements in our work and expect comparable results for other diamagnetic salt solutions.

Moreover, by tuning the magnetic field B_0 and thereby the NV-center’s Larmor frequency $\text{NV}_{0,-1}$ (i.e., the $m_s = 0 \rightarrow m_s = -1$ transition frequency) we are able to map the spectral noise density. We probe water/NaCl (500 mM) solution with $\text{NV}_{0,-1}$ frequencies from 131 MHz to 2.87 GHz and observe a similar effect over the entire frequency range (see Supplementary Note 2). Consequently, the extension of the T_1 time of near-surface NV-ensembles with exposure to diamagnetic electrolyte solutions is an effect that covers a broad range of (high) frequencies (i.e., from \sim hundreds of MHz to GHz).

Additionally, in order to exclude an impact of the solvent’s physical properties (i.e., polarity) on our experiments,¹⁹ we choose typical organic solvents whose dielectric constants (κ) and chemical structure differ significantly from water ($\kappa = 80$ ⁴⁰) and probe them with relaxometry (see Supplementary Note 3). Since the T_1 time remains unaffected, we conclude that the herein described effect is not induced by the physical properties of water, but by

the diamagnetic electrolyte.

Sensitivity of T_1 Relaxometry on Electrolytes

In order to obtain information about the sensitivity of the NV-relaxometry protocol to para- and diamagnetic electrolyte solutions, we perform additional measurement series where the electrolyte concentration is increased stepwise by one order of magnitude (from 10^{-5} to 10^{-2} mM in the case of paramagnetic MnCl_2 and from 10^{-4} to 10^3 mM in the case of diamagnetic NaCl).

Paramagnetic MnCl_2 shows a stepwise T_1 decrease in micromolar concentrations reaching a decline of up to $86 \pm 10\%$ for a $10\text{ }\mu\text{M}$ solution with respect to water covering the diamond (see Figure 2a and Supplementary Note 4). Note that a further concentration increase ($> 10\text{ }\mu\text{M}$) is not measurable, as it leads to a collapse of the T_1 time. In contrast, diamagnetic NaCl shows a slight T_1 increase compared to water, which then fluctuates moderately from micromolar to lower millimolar concentrations. Importantly, a significant and gradual T_1 increase is measurable from 10 mM to 500 mM NaCl solution, where the effect saturates at $81 \pm 11\%$ with respect to water (see Figure 2b and Supplementary Note 4).

The decrease of the T_1 time with paramagnetic species (e.g., MnCl_2) is expected and well studied.^{17,25,26,30} Here, high frequency ($\sim \text{GHz}$) noise originates from magnetic dipole-dipole interactions of the NV-center’s electronic spin and the sample’s electronic spin (“spin-flips”), resulting in a decline of the T_1 time if unpaired electrons are near the sensor. On the other hand, for diamagnetic ions (e.g., NaCl) these interactions are absent as only paired electrons without a (net) magnetic moment are present. Surprisingly, here we observe a gradual extension of the T_1 time with increasing millimolar concentrations of diamagnetic NaCl solution.

Importantly, both sensitivity regimes (\sim nano- to micromolar for paramagnetic and \sim millimolar for diamagnetic species) match the typical physiological^{41,43} or (for diamagnetic electrolytes) electrochemical concentrations,⁴⁴ opening up sensing applications in cell biology

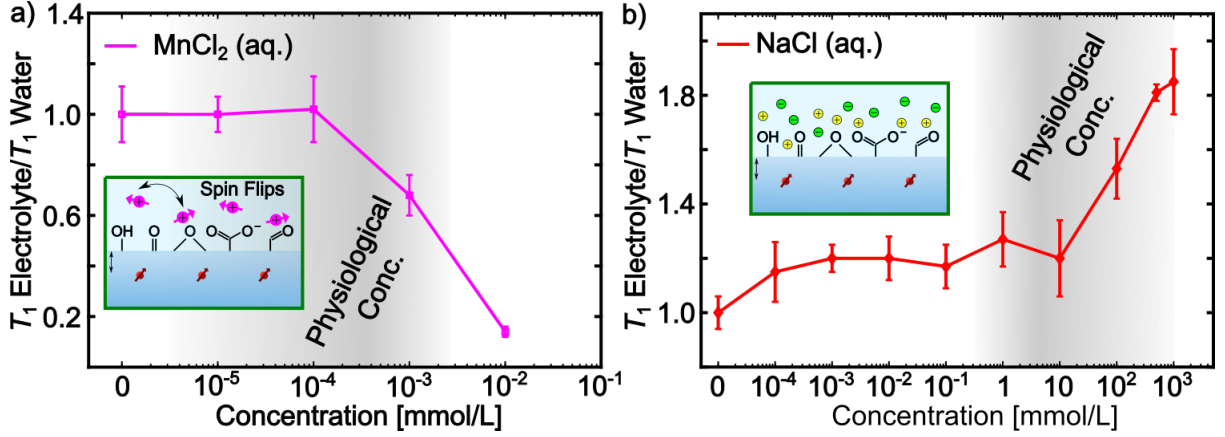


Figure 2: NV-relaxometry with increasing concentrations of para- and diamagnetic electrolyte solutions. a) Paramagnetic MnCl_2 shows a stepwise T_1 time decrease for concentrations in the micromolar regime until the effect reaches a maximum measurable decline of $86 \pm 10\%$ for $10 \mu\text{M}$ solutions with respect to water covering the diamond. b) In contrast to that, diamagnetic NaCl (right) shows a slight increase of the T_1 time compared to water, which then fluctuates moderately from the micromolar to the lower millimolar regime. For concentrations $\geq 10 \text{ mM}$ the T_1 time increases gradually along with the NaCl concentration until the effect saturates to $81 \pm 11\%$ for NaCl (500 mM) solutions. Shaded areas indicate typical physiological concentration regimes for para- and diamagnetic ions.^{41–43} Experiments are performed at $f_{\text{NV}} = 1.88 \text{ GHz}$.

or electrochemistry.

Reversibility, Passivation and NV-Center Depth

Because of the surprising observation, that the T_1 time increases with diamagnetic electrolyte solutions compared to water covering the diamond, the next experiments concentrate on the mechanism behind this effect. Therefore, we probe the reversibility and passivation of the effect along with the sensor’s response in dependence of its implantation depth. First, we evaluate if the extension of the T_1 relaxation time is a reversible process by exposing an oxygen-terminated diamond alternately to water and NaCl (500 mM) solution. Thereby, we show that the T_1 relaxation time is altered from “short” in case of water exposure to “long” when NaCl solution covers the surface (see Figure 3a in green). Alternating between water and electrolyte solution demonstrates a 1.83 ± 0.35 fold increase of the T_1 time with electrolyte exposure on the oxygen-terminated diamond. In a next step, we examine if the effect is specific to the diamond surface termination. Therefore, the formerly oxygen-terminated diamond is coated with an aluminium oxide (Al_2O_3) thin film (thickness ~ 1 nm)¹³ prepared by Atomic Layer Deposition (ALD). The aluminium oxide thin film ensures a controllable and uniform surface termination with hydroxyl groups. We repeat the previous experiment, but this time the T_1 relaxation time remains unaffected by the NaCl solution (see Figure 3a in black).

Additionally, we investigate if the extent of the electrolyte’s effect is dependent on the depth of the embedded NV-center ensemble. Therefore, we prepare two diamonds with ^{15}N implantation energies of 2.5 and 4 keV with the tri-acid clean procedure described before and probe them with NV-relaxometry. Near-surface NV-centers implanted with an energy of 2.5 keV are mainly distributed within a depth of ~ 5 nm below the surface, while ensembles created with 4 keV ^{15}N are located about ~ 12 nm beneath the surface.³⁷ Figure 3b shows a significantly larger effect of the electrolyte on the relaxation time of the shallow implanted NV-diamond with respect to the deeper one, although a T_1 time extension is still detectable in the latter case (see also Supplementary Note 5). Importantly, while the effect with the ~ 1 nm thick aluminium oxide layer is completely passivated, a T_1 time increase can still be

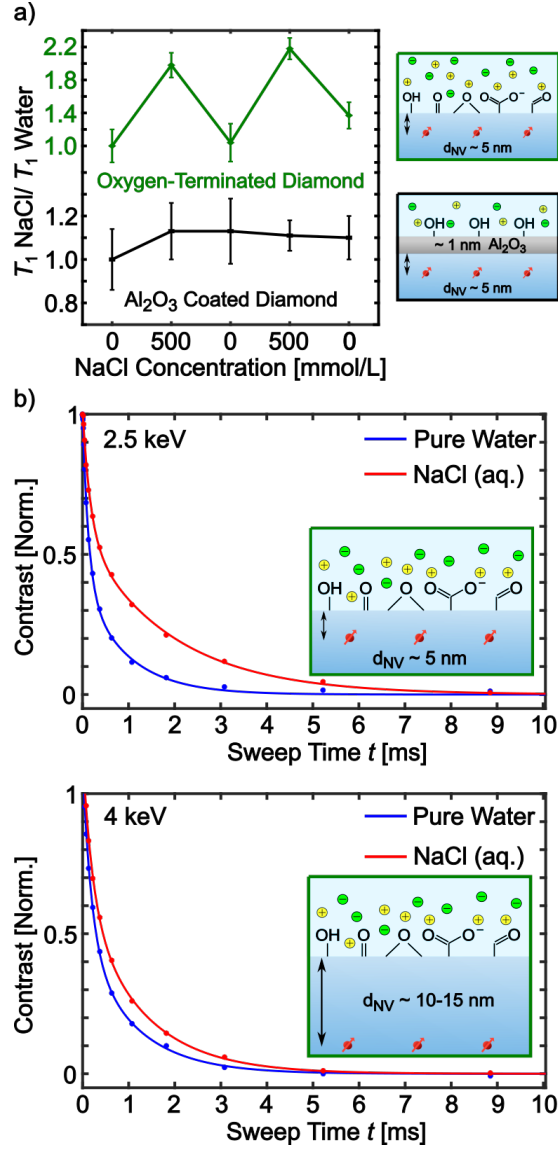


Figure 3: **NV-relaxometry experiments with different surface terminations and NV-center ensemble implantation depths.** a) An oxygen-terminated diamond surface is alternately exposed to water and NaCl (500 mM) solution. The T_1 time increases with electrolyte exposure by a factor of 1.83 ± 0.35 with respect to water. Importantly, this behavior can be altered by either the presence or absence of water or NaCl solution. After coating the same diamond with an aluminium oxide (Al₂O₃) thin film (thickness ~ 1 nm) the T_1 time is unaffected by the NaCl. b) T_1 relaxation curves of water and NaCl (500 mM) solution covering the diamond surface. Diamonds were implanted with ^{15}N at an energy of 2.5 keV (top) and 4 keV (bottom) resulting in different NV-center ensemble depths (d_{NV}). While on the shallower implanted diamond the T_1 time increases by a factor of around two with exposure to NaCl solution, on the deeper implanted diamond the effect is strongly reduced. Experiments are performed at $f_{\text{NV}} = 1.88$ GHz.

observed with the oxygen-termination when the sensor is ~ 5 to 10 nm further away from the electrolyte. Note that the same measurements conducted with LiCl (500 mM) solution lead to similar results (see Supplementary Note 5).

From these experiments we conclude that the extension of the T_1 relaxation time is a reversible and interfacial process which is dependent on the distance of the sensor to the sample.

Additionally, NV-charge state alterations or changes in NV-dephasing and NV-coherence are not observed in our experiments (see Supplementary Note 6).

Probing Magnetic and Electric Noise Contributions

In the next set of experiments we investigate if the T_1 relaxation time increase originates from a reduction of electric and/or magnetic field noise. Since we are dealing with electrolytes dissolved in water, it is particularly interesting to explore the influence that charged ions and their randomly fluctuating electric fields might have on the T_1 relaxation time of the near-surface NV-ensembles. Whereas the typically used relaxometry experiments use single quantum (SQ) transitions to probe magnetic field noise (as in the experiments from the previous sections), double quantum (DQ) transitions are influenced by electric field noise.⁴⁵ For these transitions, the full NV-center ground state ($S = 1$) is considered, where an additional relaxation pathway between $m_s = -1 \leftrightarrow m_s = +1$ with $\Delta m_s = 2$ (see Figure 4a) becomes accessible, the DQ transition. Regarding the NV-center as a “qutrit” rather than a qubit allows to probe the effect of the diamagnetic electrolyte solution on both electric and magnetic field noise at the same time.

SQ and DQ relaxometry measurements on the system water/NaCl (500 mM) solution reveal that the diamagnetic electrolyte has an effect on both relaxation channels, i.e., it reduces magnetic as well as electric field fluctuations (see Figure 4b). Here, two different T_1 times can be defined: $T_{1,\text{SQ}}$ for the relaxation time in the SQ and $T_{1,\text{DQ}}$ in the DQ channel. An extension of $T_{1,\text{SQ}}$ by a factor of 1.52 ± 0.16 and a 2.84 ± 0.31 increase of $T_{1,\text{DQ}}$ can

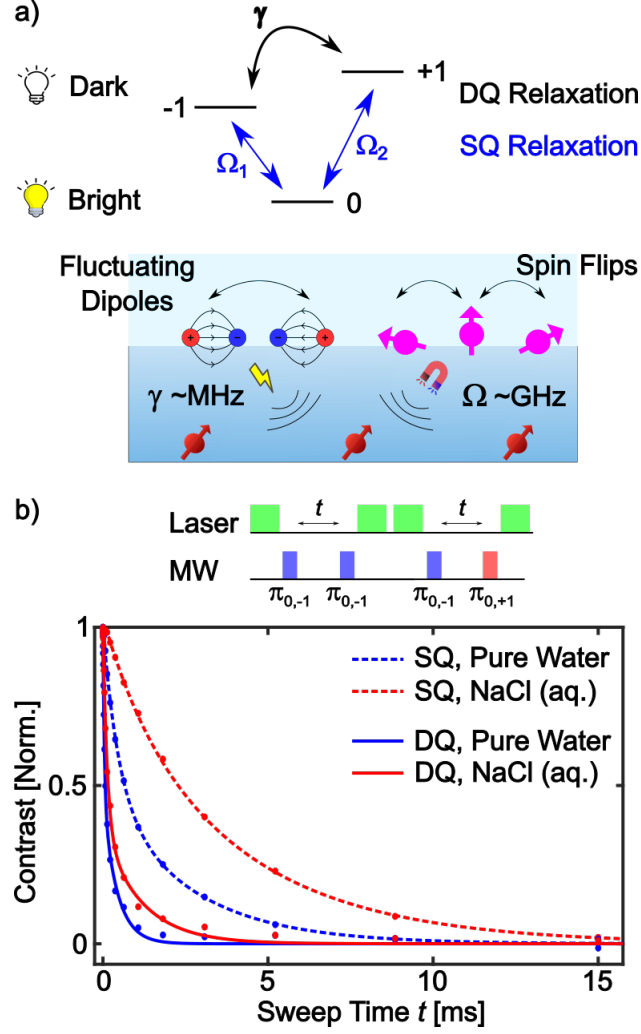


Figure 4: **Single quantum (SQ) and double quantum (DQ) relaxation experiments.** a) Energy level scheme of the NV-center ground state transitions. SQ transitions ($\Delta m_s = \pm 1$) with relaxation rates Ω are susceptible to magnetic noise. The DQ relaxation ($\Delta m_s = \pm 2$) with relaxation rate γ is magnetically forbidden but susceptible to electric noise.⁴⁵ b) Top: DQ pulse sequence. Bottom: SQ and DQ relaxation curves of water and NaCl (500 mM) solution covering the diamond. Experiments are performed at $B_0 = 15$ G, where the $\text{NV}_{0,-1}$ transition is at $f_{\text{NV}} = 2.83$ GHz (corresponding to a DQ transition frequency of 80 MHz). $T_{1,\text{SQ}}$ increases by a factor of 1.52 ± 0.16 and $T_{1,\text{DQ}}$ by a factor of 2.84 ± 0.31

when the diamond is exposed to NaCl solution.

be measured in presence of NaCl solution with respect to water (see also Supplementary Note 7). Thus, diamagnetic electrolytes reduce both – electric and magnetic – noise at the diamond surface. Importantly, when we repeat the same experiments with paramagnetic MnCl_2 , only $T_{1,\text{SQ}}$ reduces by 80%, whereas the DQ transition remains unaffected compared to water (see Supplementary Note 7). This indicates an exclusive impact of the paramagnetic electrolyte on magnetic field noise and could provide a possible pathway to distinguish para- from diamagnetic ions in solution.

Additionally, we can exclude an influence of diamagnetic NaCl solution on the static electric field environment by performing zero field ESR Measurements (see Supplementary Note 7).

Influence of Electrolytes on Surface Dark Spins: DEER Experiments

So far, we have focused on the direct influence of electrolytes on the NV-centers. However, the diamond as the NV-center’s host material provides various surface dark spins, e.g. dangling bonds, whose response to the electrolytes is probed in the next set of experiments. Intrinsic T_1 times of these surface dark spins are often long (\sim a few microseconds)⁴⁶ which allows us to probe them with NV-based double electron electron resonance (DEER) spectroscopy.^{16,47} Figure 5a shows the pulse sequence of a typical DEER experiment: A spin-echo is performed on the NV-center’s electronic spin ($\text{MW}_{\text{NV spin-echo}}$), at the same time, in the second free precession time of the echo, an additional microwave pulse (MW_{DEER}) is applied to drive the target electronic spins. Sweeping the MW frequency (f_{DEER}) flips the surface dark spins when their Larmor frequency is matched and causes a dip in the DEER signal (see Figure 5b). As shown in Figure 5b, a clear dip in the DEER spectrum appears when the diamond interface is covered with NaCl (500 mM) solution. The resonance at $f_{\text{DEER}} = 0.887 \text{ GHz}$ corresponds to $g_e \sim 2$ spins and is typically assigned to dangling bonds at the diamond surface.⁵⁰ Interestingly, the dip is drastically reduced when the experiment

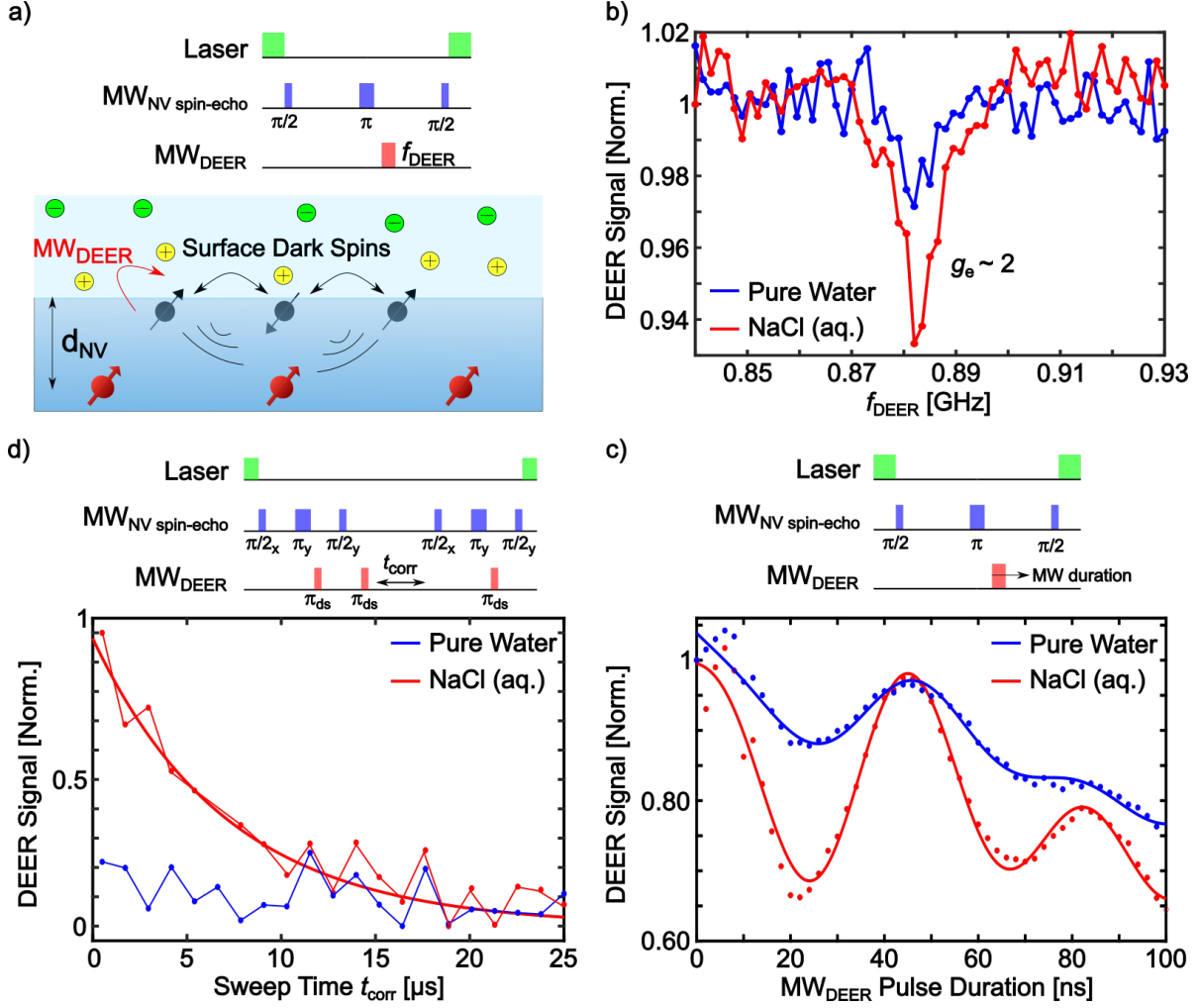


Figure 5: NV-DEER experiments probing the response of surface dark spins to electrolyte exposure. a) Pulse sequence of the double electron electron resonance (DEER) experiment. Sweeping the microwave frequency of the MW_{DEER} pulse (f_{DEER}) while applying a spin-echo experiment on the NV-center ($MW_{\text{NV spin-echo}}$) allows for the detection of electronic (surface dark) spins coupled to the NV-centers.⁴⁸ b) DEER experiment with water and NaCl (500 mM) solution covering the diamond surface. A pronounced dip in the DEER spectrum appears at around 0.887 GHz (where $g_e \sim 2$) when the diamond is exposed to NaCl solution. The dip gets drastically reduced when water covers the diamond surface. c) Top: Pulse sequence of the DEER-Rabi experiment. Bottom: When the pulse duration of the microwave drive (MW_{DEER}) at the surface dark spins' resonance frequency is swept during the spin-echo, DEER-Rabi oscillations can be observed.⁴⁹ While the π_{ds} -pulse lengths remain equal when water or NaCl (500 mM) solution cover the diamond surface ($\pi_{\text{ds}} \sim 24$ ns), the latter causes a by a factor of around three more pronounced Rabi amplitude. d) Top: Pulse sequence of the DEER- T_1 experiment. Bottom: Varying the correlation time (t_{corr}) between two subsequent DEER segments,⁴⁶ shows a surface dark spin relaxation with $T_{1,\text{ds}} = 7.20 \pm 1.10$ μs in case of NaCl exposure. In contrast, no significant relaxation decay can be observed when water covers the diamond surface. DEER experiments are performed at $f_{\text{NV}} = 1.98$ GHz.

is repeated with water.

Once the resonance condition for the $g_e \sim 2$ spins is found, coherent control of the surface dark spin state can be demonstrated. Figure 5c shows a DEER-Rabi experiment on the surface dark spins. Sweeping the microwave pulse duration (MW_{DEER}) during the spin-echo causes oscillations of the defect’s spin state.⁴⁹ While we determine equal π_{ds} pulse lengths ($\pi_{\text{ds}} \sim 24 \text{ ns}$) for water and the electrolyte, the former leads to an about three times increased DEER-Rabi amplitude with respect to the latter. In the next step, we probe the surface dark spin relaxation time ($T_{1,\text{ds}}$). Figure 5d depicts a pulse sequence from Sushkov *et al.*,⁴⁶ where the T_1 time of the surface dark spins can be measured by correlating two subsequent DEER segments and varying the correlation time t_{corr} . Interestingly, we measure a relaxation time $T_{1,\text{ds}}$ of $7.20 \pm 1.10 \mu\text{s}$ for the surface dark spins exposed to the NaCl solution. In contrast, a clear relaxation decay cannot be observed in case of pure water covering the diamond. Although we cannot exclude that the surface dark spins vanish, the more likely case is that the dark spins act as reporter spins⁴⁶ experiencing the same effect of the electrolyte solution as the NV-center: “fast” relaxation in the case of water and “slow” relaxation when diamagnetic electrolyte solutions cover the diamond, which is also expressed in the increased DEER signals (see Figure 5b-d). Accordingly, we enhance the sensitivity of our sensor by the proximity of the reporter spins to the electrolyte solutions.^{46,51}

Theoretical Modeling

Our experimental results show an influence of diamagnetic electrolyte solutions on near-surface spin defects in diamond where electric as well as magnetic noise is suppressed resulting in an increase of the T_1 relaxation time. To further study this surprising effect computational modeling is used. Here, as a working assumption, we focus on charge fluctuations within the diamond lattice. We note, that further processes such as proton hopping at the interface or water and ion dynamics within the electric double layer can also play a role but have not

been treated herein.

To this end, we model an interface between a slab of diamond and a thin layer of water subsequently enriched by Na^+ and Cl^- ions (see Methods for detail). Then, we probe the interfacial structure and vacuum level shifts (VLS) based on the configurations obtained from the *ab initio* molecular dynamics (MD)(see Figure 6a). The calculated alignment of the electronic levels of water and the model diamond surface is shown in Figure S10. Here, a mismatch of the chemical potentials (defined as a center of the band gap) promotes an electron leakage from the diamond surface towards the water. The resulting redistribution of charges leads to the development of an electric field, that further rearranges the charged solvated Na^+ and Cl^- ions. The large positive VLS of 1.1 eV (see Figure S10a) causes the ions to rearrange with the direction of the field, facilitating the effect of band bending. By adding a carboxyl group, we observe a stabilization of the downwards band bending relative to the case of the model diamond surface in water. However, in both cases, we obtain a broad distribution of surface dipoles, owing to the complexity of ion dynamics within the Stern layer. By contrast, a sharp distribution of the dipole moments is observed between a dissociated carboxyl group and a solvated Na^+ ion nearby. This stable configuration gives rise to a large VLS of ~ -1.9 eV. This value is further used to trace the evolution of the electrostatic potential at the microscopic level. More specifically, we set it as a boundary condition for solving the Poisson equation to access the modifications of the potential inside a semi-infinite diamond slab. As shown in Figure 6b, we observe that the interfacial region of ~ 40 nm is affected by the respective readjustments of the charges, resulting in a rapid decay of the potential near the interface and a slow saturation towards the bulk.

To establish a relation between the band bending and the noise reduction, we consider the electric and magnetic fluctuations caused by a pair of active defects around the NV-centers. The charge transfer process leads to a continuous change in the charge/spin state of the nearby defects, which can affect the relaxation and coherence time of the NV-center when the rate approaches the timescale of the quantum sensing experiment. In the Marcus theory,

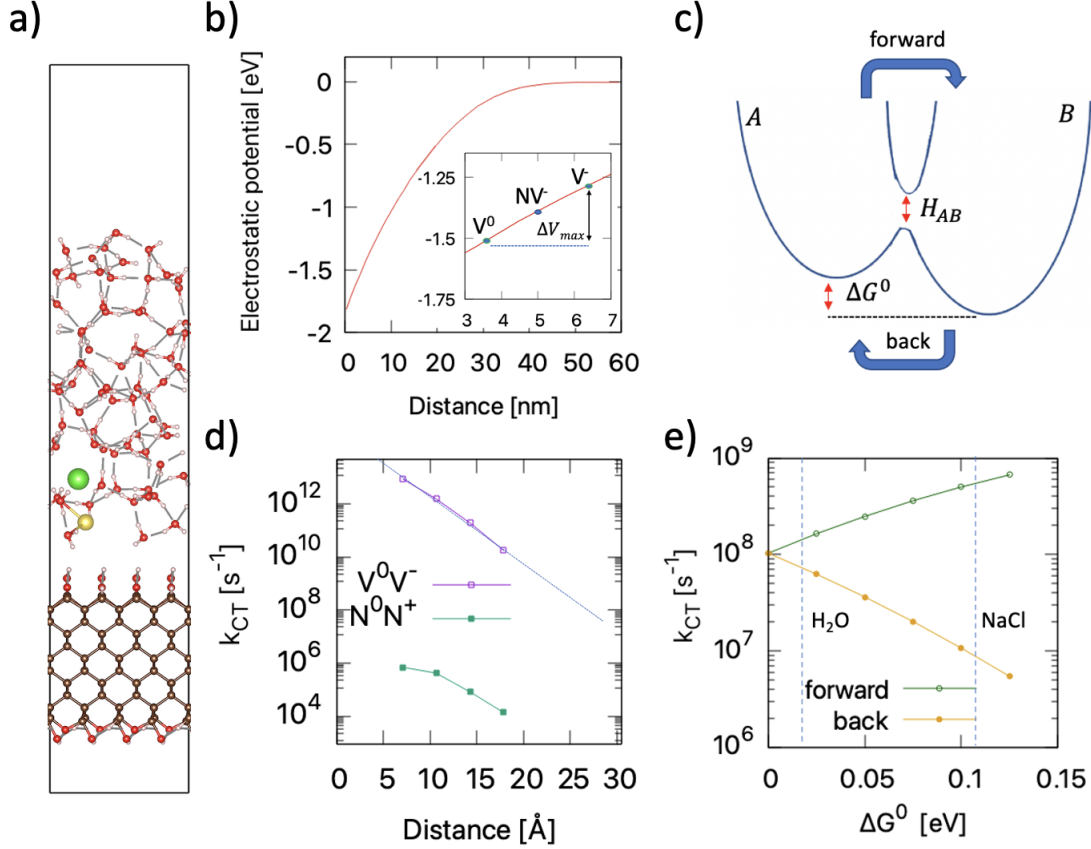


Figure 6: ***Ab initio* MD simulations of the diamond/electrolyte interface.** a) Representative snapshot of the diamond/electrolyte interface from the *ab initio* MD simulations. Color code: C (grey), O (red), H (white), Na⁺ (yellow), Cl⁻ (green). b) Variations of the electrostatic potential in a semi-infinite diamond due to the arrangement of NaCl at the interface. Inset: Electrostatic potential (ΔV_{\max}) for a pair of defects in 3 nm distance to each other surrounding a ~ 5 nm deep NV-center. c) Schematic representation of a continuous charge hopping between two defects around the NV-center. H_{AB} is the transfer integral, ΔG^0 is calculated as $\Delta V_{\max}/2$ from b). d) Calculated rate constants for pairs of substitutional nitrogen and vacancy defects as a function of distance between the defects. e) Rate constants for the forward and backward electron transfer between a pair of vacancy defects as a function of bias due to the interfacial band bending. Vertical lines refer to an estimated difference in the effects by replacing the electrolyte with pure water, considering a pair of defects and a NV-center in a configuration from the inset in b).

such fluctuations are described as a sequence of thermally activated hopping events, whilst the rate constants are determined from the distance-dependent coupling parameters and the required structural reorganizations (see Figure 6c). The dipoles at the diamond/solvent interface affect this equilibrium by altering the onsite Gibbs energy term with a contribution from the electrostatic potential (ΔV). As shown in Figures 6c and 6e, the band bending accelerates a forward charge transfer process (until reaching the Marcus inverted region), but at the same time, the magnitude of the back charge transfer (BCT) rate drops exponentially. Hence, regardless of the defect type, large interfacial band bending can lead to a dynamical trapping of the charges around a site with the lower Gibbs energy. For a numerical validation, we focus on the electron fluctuations between a pair of carbon vacancies as well as on the hole fluctuations between two substitutional nitrogen defects. We note that carbon vacancies are often generated by the implantation and irradiation techniques used to create the NV-centers, and substitutional N defects are present around NV-centers to stabilize the negative charge state of the NV-center. After determining the relevant parameters in the periodic supercells (see Methods for detail), we first analyze the possible contribution of each charge transfer reaction to the electrical noise. To this end, we compare the fluctuation rates, calculated for both defect pairs in a bulk-like environment ($\Delta V = 0$). As shown in Figure 6d, the charge fluctuation rates for a pair of nitrogen defects is remarkably smaller than for a vacancy pair. This difference is attributed to a formation of an energetically unfavorable N^0 configuration, that hinders the charge fluctuations by large structural reorganizations ($\lambda_{\text{reorg}} = 1.89 \text{ eV}$). Hence, substitutional N^0 pairs are unlikely to be the origin of electric and magnetic noise, affecting the T_1 time due to charge fluctuation. By contrast, owing to a rather modest λ_{reorg} of 0.28 eV, a vacancy pair gives rise to noise in a broad frequency range, where the respective rate constants are controlled by the separation between the active sites.

The relevant distance between a pair of vacancies is readily obtained from an exponential fit of the rate constants in Figure 6d. More specifically, we find the charge fluctuation rates, which would be relevant for an influence on the T_1 time ($\sim 0.1 \text{ GHz}$) at a separation of \sim

3 nm. The molecular dynamics simulations performed by Fávoro de Oliveira *et al.* show that such a high local density of vacancies around the region of a NV-center is achieved during the nitrogen implantation due to the cascade process of the “kick-out” mechanism.⁵² Using the variations of electrostatic potential from Figure 6b for the implantation depths of 5 and 12 nm, we calculate a contribution to the onsite Gibbs energies by 0.125 and 0.075 eV, respectively (see Methods for details). As shown in Figure 6e, the BCT rate at 12 nm reduces by a factor of ~ 7 relative to the case of $\Delta V = 0$. Moreover, in agreement with our experimental results, the faster changes in the potential at 5 nm enhances the reduction factor to ~ 19 for the shallower NV-centers. Relative to pure water, the BCT rates decrease by factors of ~ 10 and 3.5 for the depths of 5 nm and 12 nm, respectively. Furthermore, the proposed mechanism is consistent with the experimental results on dark spins (see Figure 5). Interestingly, our calculations point to an even larger decrease of the BCT rate at smaller distances from the interface which should translate to an even larger sensitivity. Given the favorable downwards band bending, these results call for a further optimization of the implantation parameters as well as the surface structure to fully exploit the extension of the T_1 time by diamagnetic electrolyte solutions.

Conclusion and Outlook

We report on the effect of diamagnetic electrolyte solutions on highly dense near-surface spin defects in oxygen-terminated diamonds. Surprisingly, we observe that diamagnetic ions increase the T_1 relaxation time of NV-centers. We demonstrate that this effect is reversible, surface sensitive and responsive to millimolar concentrations. We find that also interfacial spin defects are sensitive to diamagnetic species, anticipating their possible use as reporter spins for future optimization. Furthermore, we investigate the underlying mechanism by single and double quantum NV-relaxometry experiments in combination with *ab initio* simulations. We propose that ions at the interface stabilize charge fluctuations between pairs of

carbon vacancies and alike deep defects, surrounding the NV-centers. This reduces magnetic as well as electric noise at the diamond interface by a dynamical trapping of mobile electrons to a site with lower Gibbs energy. These findings encourage further simulations and experiments (e.g, on other NV-diamond systems, such as nanodiamonds or single NV-centers) to elaborate on a comprehensive understanding of the complex processes at the solid/liquid interface.

We would like to emphasize that the sensitivities of relaxometry to para- and diamagnetic electrolyte solutions both represent scientifically relevant concentration regimes. Paramagnetic species in the physiological environment, e.g., reactive oxygen species (ROS) or trace metals, e.g., manganese can typically be found in \sim nanomolar to micromolar concentrations fitting the highly sensitive feedback of NV-relaxometry (see Figure 2a).^{41,53} However, diamagnetic ion concentrations are typically orders of magnitude higher in the cytoplasm (\sim millimolar)^{42,43} or in electrochemistry (\sim 0.1 to 1 molar)⁴⁴ which fit very well the NV-center’s response reported in our work (see Figure 2b). Importantly, these two effects may counteract if both species are present. A possible pathway to differentiate between these two could be recording single *and* double quantum experiments, which are only affected by diamagnetic species in the latter case (see Figure 4 and Supplementary Note 7). Therefore, we propose to probe both relaxation times in future relaxometry studies. We envision applications ranging from probing electrochemical interfaces⁵⁴ to nanoscale ion sensing in cells or neuroscience, where changes in the membrane potential occur as a result of concentration gradients of diamagnetic ions.^{55–57}

Methods

Sample Preparation

Two $2 \times 2 \times 0.5$ mm electronic grade diamond samples (natural ^{13}C abundance, Element Six) were implanted with ^{15}N at an energy of 2.5 keV or 4 keV, an off-axis tilt of 7° and a

fluence of $2 \times 10^{12} \text{ cm}^{-2}$ by Innovion and annealed according to Bucher *et al.*¹⁸ Before experiments are conducted, the diamonds are cleaned with a tri-acid cleaning protocol according to Brown *et al.*:³⁸ Samples are boiled in equal parts of sulfuric, nitric and perchloric acid at a temperature of 280 °C for two hours. This cleaning procedure is also applied before the deposition of aluminium oxide (Al_2O_3) on the diamond.

Preparation of Electrolyte Solutions

For the measurements where pure water is used, deionized water with a resistivity of 18.2 M Ω ·cm at 25 °C (Merck Millipore) is utilized.

Sodium chloride (NaCl, Merck 106404) is prepared in a 1 M stock solution, where NaCl is dissolved in deionized water. Before the experiments, NaCl is diluted from the stock solution to obtain 500, 250, 100, 50, 10 and 1 mM concentrated solutions. The other salt solutions used within this work are prepared in the same manner.

Atomic Layer Deposition (ALD)

The 2.5 keV ^{15}N implanted diamond is coated with an aluminium oxide (Al_2O_3) thin film by ALD according to Liu *et al.*¹³ The deposition includes 10 cycles of alternated sample exposure to trimethyl aluminium (TMA) and H_2O . This procedure results in a film thickness of $\sim 1 \text{ nm}$ and ensures surface termination with hydroxyl groups by exposing the diamond to a remote oxygen plasma within the ALD system.^{13,58} The Al_2O_3 layer can be removed from the diamond surface by soaking the sample overnight in 5% NaOH solution.

Experimental Setup

The quantum sensing setup is based on a modified version of the experiment described in Bucher *et al.*¹⁸ Before experiments are performed, the diamond is glued to a thin glass cover slide (48393026, VWR) together with a microfluidic device that encloses the diamond

edges and covers its surface, such that a volume of $\sim 0.60\text{ }\mu\text{L}$ of the sample liquid can be applied in a controllable way. On the other side of the cover slide a 6 mm diameter glass hemisphere (TECHSPEC[®] N-BK7 Half-Ball Lenses, Edmund Optics) is glued, in order to improve the fluorescence light collection efficiency. The glass cover slide is then fixed on a 30 mm cage plate (CP4S, Thorlabs). This whole assembly is then positioned between two permanent magnets, that are rotated and tilted in order to align the B_0 field with one of the four possible NV-center orientations. The distance between the two magnets can be adjusted in order to correspond to the working magnetic field strengths B_0 (in this work: 15, 316, 352 and 978 G). Initialization of the NV-ensemble is realized with a 532 nm laser (Verdi G5, Coherent) with a power of $\sim 250\text{ mW}$ (CW) after the AOM. The laser light is focused on the diamond by a Plano-Convex Lens (LA 1986-A-M, Thorlabs) in a total internal reflection geometry. Laser pulses are regulated by an acousto-optic modulator (Gooch and Housego, model 3260-220) with pulse durations of 5 μs . Photoluminescence (PL) is collected and focused on a large area photodiode (OE-300-SI-10, Femto Messtechnik GmbH, Berlin, Germany) by two condenser lenses (ACL25416U-B, Thorlabs). The excitation light is filtered by a long-pass optical filter (Edge Basic 647 Long Wave Pass, Semrock) placed between the bottom condenser lens and the photodiode. The output voltage of the photodiode is digitized with a data acquisition unit (USB-6229 DAQ, National Instruments). A 500 MHz PulseBlaster card (ESR-Pro-II, Spincore) is utilized to trigger and to time the microwave and light pulses used for quantum control of the NV-centers. The microwave frequencies are produced by a signal source (SynthHD, Windfreak Technologies, LLC.). Microwave phase control is obtained by a combination of a phase-shifting splitter (ZX10Q-2-27-S+, Mini-Circuits), two switches (ZASWA-2-50dRA+, Mini-Circuits) and a combiner (ZX10-2-42-S+, Mini-Circuits). The amplified microwave pulses (ZHL-16W-43-S+, Mini-Circuits) are delivered by a homebuilt microwave loop on top of the microfluidic chip. The electron spin resonance (ESR) frequency is used to determine the magnetic field strength B_0 as well as the $\text{NV}_{0,-1}$ resonance frequency f_{NV} .

T_1 Relaxometry Experiments (Single and Double Quantum)

Single quantum (SQ) relaxometry experiments: To obtain a signal-to-noise ratio (SNR) as shown in Figure 1b the sequence is repeated 5,000 times for every data point. Each experiment consists of 31 data points measured in a logarithmic increasing sweep time t to guarantee more sampling points at short times t . Note that these parameters are also used for double quantum (DQ) relaxometry. For normalization and noise cancellation, the second half of the sequence contains a MW $\pi_{0,-1}$ -pulse, where the subscripts 0 and -1 indicate the initialization of the spin state from $m_s = 0$ to $m_s = -1$.¹⁸ The spectra are then plotted as the measurement result of the first half divided by the result of the second half of the sequence.

Double quantum (DQ) relaxometry experiments: For a detailed discussion of the DQ relaxation and pulse sequence, the reader is referred to Myers *et al.*⁴⁵ In short, the DQ pulse sequence (see inset of Figure 4b) consists of two consecutive measurements where MW π -pulses are used to control spin state initialization and readout. In both halves of the sequence the NV-center is initialized in $m_s = -1$. After a sweep time t the spin state population of either $m_s = -1$ (in the first part) or $m_s = +1$ (in the second part) is read out. Dividing the second by the first part yields a population ratio of the two states.

Sensitivity of T_1 Relaxometry on Electrolytes

Experiments to determine the sensitivity of T_1 relaxometry measurements on para- and diamagnetic electrolytes are conducted for MnCl_2 and NaCl solutions using the SQ relaxometry pulse sequence. Probing each concentration results in a relaxation curve of which the T_1 time is determined. The T_1 time is then normalized to the one of water covering the diamond. Before probing any electrolyte concentration, we wash the microfluidic device with water to ensure equal starting conditions, i.e. a constant T_1 time for water covering the diamond. We perform each series three times resulting in a mean T_1 value for each concentration (see also Supplementary Note 4). Figure 2 in the main text shows the mean

(normalized) T_1 time along with the standard deviation.

DEER Measurements

DEER spectra (see Figure 5b) are recorded by performing a spin-echo sequence on the NV-center spins with a free evolution time of 1 μ s. The duration of the MW-pulse (MW_{DEER}) applied to the surface dark spins is set to 200 ns and the driving frequency (f_{DEER}) is swept over 90 MHz (from $f_{\text{DEER}} = 0.84$ to 0.93 GHz). To obtain a SNR as shown in Figure 5b the sequence is repeated 10,000 times for every data point. Each experiment consists of 67 data points in equally separated time steps and this whole experiment is repeated four times. Referencing for noise cancellation is achieved by alternating the last MW-pulse of the spin-echo sequence from $\pi/2$ to $3/2\pi$.

Once the resonance condition for $g_e = 2$ is found, DEER-Rabi experiments on the surface dark spins are performed by sweeping the MW-pulse duration (MW_{DEER}) during the NV spin-echo (see Figure 5c) as described above. The sequence is repeated 10,000 times for every data point. Each experiment consists of 101 equally spaced data points and this whole experiment is repeated ten times. To account for MW (MW_{DEER}) noise, the same procedure is repeated 20 MHz off the resonance condition. The outcome of both on- and off-resonant measurements are subtracted resulting in the spectra shown in Figure 5c. After that, measurements of the surface dark spin population relaxation are carried out according to Sushkov *et al.* with a π_{ds} -pulse length of 24 ns.⁴⁶ The sequence shown in Figure 5d is repeated 10,000 times for every data point. Each experiment consists of 21 data points in equally separated time steps. This whole experiment is then repeated 50 times. Background subtraction is achieved by performing the experiment in the same procedure without the additional MW drive (MW_{DEER}). Subtracting the outcome of both MW-on and MW-off measurements then yields the spectra shown in Figure 5d.

Simulation of the Diamond/Water Interface

In our simulations, we use a slab of a model diamond surface with hydrogen, hydroxyl, and ether surface terminations (see Figure S10d). It is a symmetric (100) surface of ~ 1.4 nm with a 2×1 surface reconstruction pattern, exhibiting a positive electron affinity and no surface states inside the band gap.⁵⁹ The water layer on top of the diamond (thickness ~ 2 nm) was constructed as follows. First, we equilibrate 74 water molecules with the classical molecular dynamics (MD) for 5 ns in a simulation box of commensurate lateral size with the diamond slab. These calculations are done with the GROMACS software in the canonical NVT ensemble,⁶⁰ using the GROMOS 54A7 force field.⁶¹ After that, we superimpose the water box and the diamond surface and allow for an additional equilibration step of 10 ps with the *ab initio* MD, as implemented in the VASP package.⁶² We also incorporate ~ 1.9 nm of vacuum together with a dipole correction scheme to eliminate the interaction with the periodic images. This yields the simulation supercell of $1.0097 \times 1.0097 \times 5.3$ nm³, which is further used in the *ab initio* MD calculations. *Ab initio* calculations are performed using the PBE functional⁶³ in conjunction with the D2 dispersion correction, using a projector augmented wave method with the kinetic energy cutoff of 370 eV. We note that the PBE functional provides semi-quantitative results for the electronic structure but is able to accurately yield the trends in the change of the electronic structure upon different surface terminations and environments of diamond. Further, we note that we focus on the difference in the electrostatic environment due to the interaction of the electrolyte with the surface groups, assuming no change in the microstructure of the carbon layer.

Charge Transfer Rates

We calculate the charge transfer rate with an expression from the Marcus theory,⁶⁴ given as:

$$k_{CT} = \frac{2\pi}{\hbar} |H_{AB}|^2 \frac{1}{\sqrt{4\pi\lambda k_B T}} \exp\left(-\frac{(\lambda + \Delta G)^2}{4\pi\lambda k_B T}\right)$$

where H_{AB} is the transfer integral, λ the reorganization energy, ΔG the Gibbs energy difference due to an external field, k_B the Boltzmann constant, \hbar the reduced Planck constant, and T the temperature. The reorganization energy is determined for a single defect (either a carbon vacancy or a substitutional nitrogen) in a 1000-carbon supercell. For computing the transfer integrals as a function of distance, we use diamond supercells of different sizes, varying between 64 and 1000-carbon atoms. The reorganization energies are calculated by the four-point scheme, while the transfer integrals are estimated at a high symmetry configuration as 1/4 of the bandwidth along the Γ -X direction. The contribution to the Gibbs energy is computed by solving the one dimensional Poisson equation given the experimental depth of the NV center.⁶⁵ Noteworthy, the effect from the band bending is governed by the orientation of defect pairs relative to the direction of the electric field. At a reference depth of the NV-center, the maximum strength, corresponding to a change in the electrostatic potential (ΔV_{max}), is reached in a parallel configuration, whilst the effect is quenched towards the orthogonal arrangement. Considering a uniform distribution of the defects in our samples, we compute an expectation value of ΔV as $\Delta V_{\text{max}}/2$.

Acknowledgement

This study was funded by the Deutsche Forschungsgemeinschaft (DFG, German Research Foundation) - 412351169 within the Emmy Noether program. R.R. acknowledges support from the DFG Walter Benjamin Programme (Project RI 3319/1-1). D.B.B. acknowledges support from the DFG under Germany's Excellence Strategy—EXC 2089/1—390776260 and the EXC-2111 390814868. M.S.B. acknowledges support from the DFG through the Munich Center of Quantum Science and Technology (MCQST, EXC-2111) and by BMBF (epiNV, 13N15702). A.G. acknowledges the Hungarian NKFIH grant No. KKP129866 of the National Excellence Program of Quantum-coherent materials project, the support for the Quantum Information National Laboratory from the Ministry of Culture and Innovation of Hungary

(NKFIH grant No. 2022-2.1.1-NL-2022-00004), the EU EIC Pathfinder project "QuMicro" (grant No. 101046911) and the EU QuantERA for the project MAESTRO. We acknowledge KIFÜ for awarding us access to computational resources based in Hungary.

Author Contributions

D.B.B., R.R. and F.A.F.-M. discovered the effect of diamagnetic electrolytes on the relaxation of NV-centers. D.B.B., R.R. and F.A.F.-M. designed the experiments. D.B.B. supervised the study. F.A.F.-M. performed the experiments and was supported by M.R.S. for NV-relaxometry. F.A.F.-M., R.R. and D.B.B. analyzed the data. R.D.A. built the quantum sensing setup and designed the microfluidic device. A.G. and A.P. incorporated theoretical modeling and simulations. M.S.B. and L.M.T. helped with the charge state experiments. All authors discussed the results and contributed to the writing of the manuscript.

Additional Information

Competing interests: The authors declare no competing interests.

Data availability

The data supporting our findings are available within the paper and the Supplementary Information. Additional relevant data are available from the corresponding author upon reasonable request.

Code availability

The codes used for data acquisition and processing are available from the corresponding author upon reasonable request.

Supplementary Information

Supplementary Note 1: Fitting of T_1 Single Quantum (SQ), Double Quantum (DQ) and Surface Dark Spin Relaxation Curves

Recorded single quantum (SQ) and double quantum (DQ) relaxation curves are fitted with a biexponential function as the T_1 decay exhibited two components according to prior work:^{25,27,28,32,66}

$$C(t) = A \cdot \exp\left(-\frac{1}{T_{1a}} \cdot t\right) + (1 - A) \cdot \exp\left(-\frac{1}{T_{1b}} \cdot t\right)$$

where C is the contrast, A is the amplitude and $T_{1a} \gg T_{1b}$. For completeness, relaxation times in the tables are given by both time constants. In agreement with prior work,^{25,27,32} values of T_1 in the main text are only considering the longer component T_{1a} . However, both time constants are longer in all cases where diamagnetic electrolytes are measured with NV-relaxometry and compared to water (see Table S1). Errors and errorbars from SQ and DQ relaxation curves shown in tables or figures are standard deviations from the biexponential fit function or in case of the sensitivity experiments (see Figure 2) the standard deviation from three consecutive measurements. T_1 time constants in the tables are given to three significant digits. In case of the $T_{1,ds}$ relaxation measurements (see Figure 5d), the relaxation curve is fitted to a single exponential decay: $C(t) = A \cdot \exp\left(-\frac{1}{T_{1,ds}} \cdot t\right)$.⁴⁶

Supplementary Note 2: T_1 Time Constants of Measured Electrolytes and T_1 Time Magnetic Field Dependence for Pure Water/NaCl (500 mM)

Table S1 and Figure S1 show the T_1 time constants (T_{1a} and T_{1b}) and T_1 relaxation curves of the measured electrolyte solutions in this work. Experiments are conducted with the relaxometry pulse sequence according to the main text.

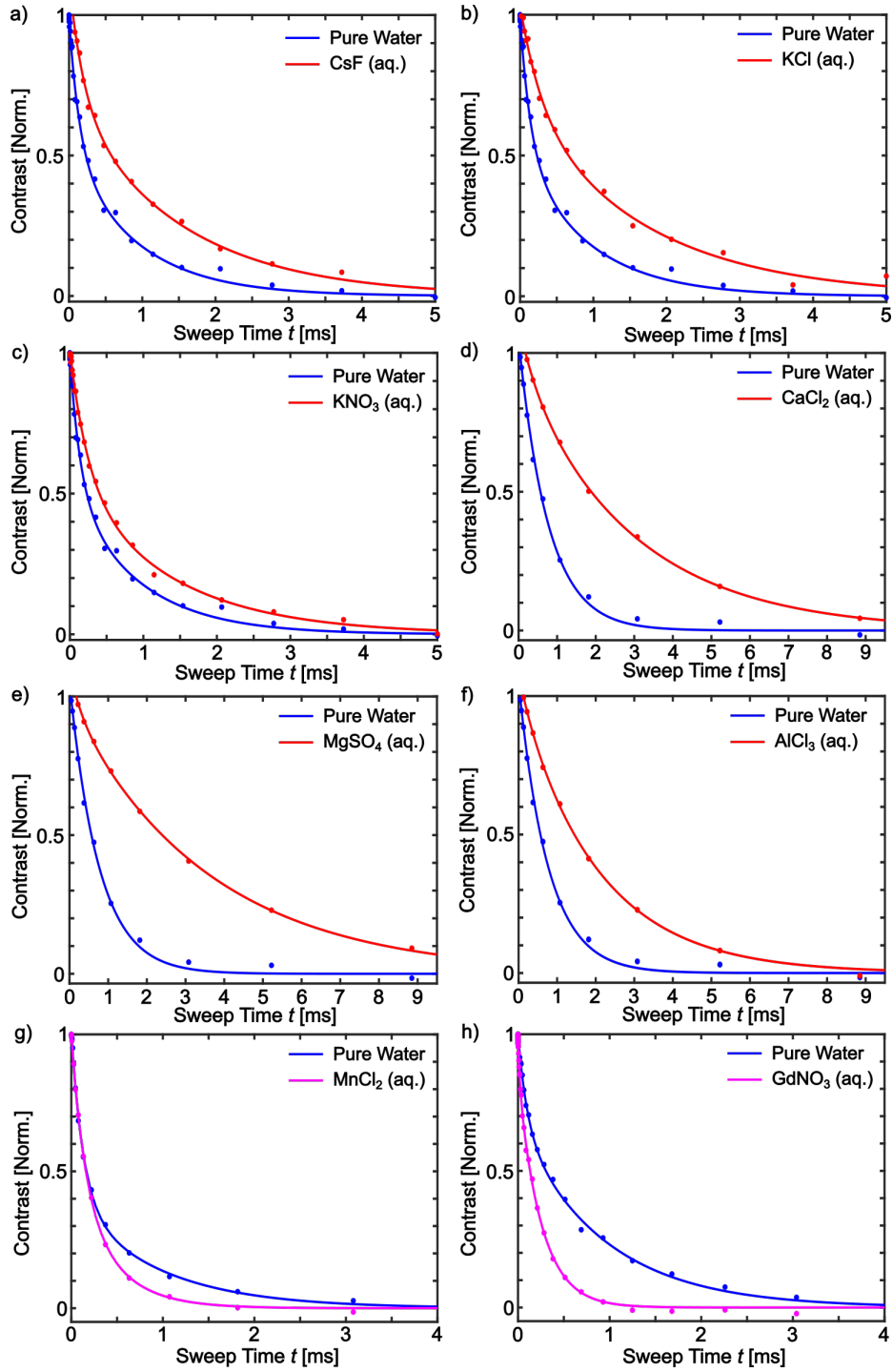


Figure S1: T_1 relaxation curves of water and a-f) diamagnetic electrolyte (500 mM) solutions as well as g) and h) paramagnetic electrolyte (1 μ M) solutions covering the diamond surface. Experiments are performed at $f_{\text{NV}} = 1.88$ GHz.

Table S1: T_1 time constants (T_{1a} and T_{1b}) of water and measured diamagnetic electrolyte solutions (500 mM) as well as paramagnetic electrolyte solutions (1 μ M) covering the diamond surface. Experiments are performed at $f_{\text{NV}} = 1.88$ GHz

Electrolyte [c = 500 mM]	T_{1a} [μ s]	T_{1b} [μ s]
Water	920 ± 170	140 ± 60.0
CsF	1510 ± 250	200 ± 60.0
KCl	1720 ± 300	270 ± 90.0
KNO ₃	1360 ± 220	240 ± 50.0
LiCl	2940 ± 720	930 ± 40.0
NaCl	1920 ± 200	170 ± 20.0
CaCl ₂	2920 ± 260	460 ± 190
MgSO ₄	3600 ± 160	310 ± 100
AlCl ₃	2070 ± 370	360 ± 190
Electrolyte [c = 1 μ M]	T_{1a} [μ s]	T_{1b} [μ s]
MnCl ₂	430 ± 160	140 ± 50.0
Gd(NO ₃) ₃	250 ± 15.0	21 ± 6.00

Further measurements of water/NaCl (500 mM) solution are performed in different magnetic fields B_0 (978, 352, 15 and 0 G), i.e., different resonance frequencies of the NV-center's $m_s = 0 \rightarrow m_s = -1$ transition ($f_{\text{NV}} = 0.131, 1.88, 2.83$ and 2.87 GHz). Figure S2 shows the T_{1a} time constants depending on f_{NV} (see Supplementary Note 1 for details). In Table S2 both time constants (T_{1a} and T_{1b}) are listed.

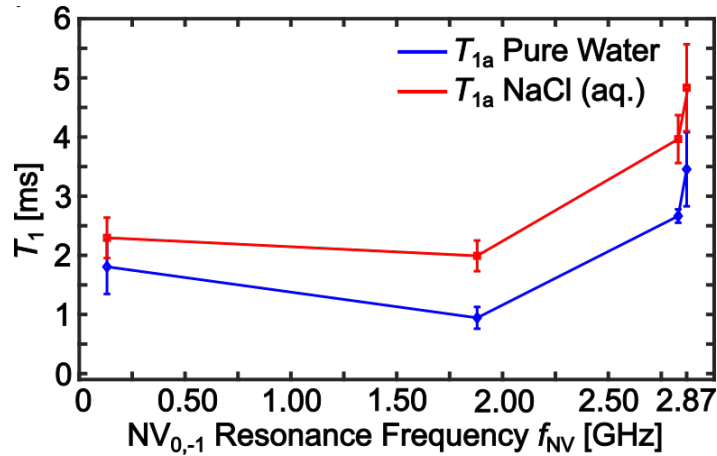


Figure S2: T_{1a} time constants for water and NaCl (500 mM) solution and their dependence on the NV_{0,-1} resonance frequency f_{NV} .

Table S2: T_1 time constants (T_{1a} and T_{1b}) for water and NaCl (500 mM) solution covering the diamond surface depending on the $\text{NV}_{0,-1}$ resonance frequency f_{NV} .

	T_{1a} [μs]	T_{1b} [μs]
$f_{\text{NV}} = 0.131 \text{ GHz}$		
Water	1810 ± 460	400 ± 60.0
NaCl 500 mM	2300 ± 340	670 ± 130
$f_{\text{NV}} = 1.88 \text{ GHz}$		
Water	940 ± 180	130 ± 20.0
NaCl 500 mM	1990 ± 200	170 ± 20.0
$f_{\text{NV}} = 2.83 \text{ GHz}$		
Water	2660 ± 110	510 ± 80.0
NaCl 500 mM	3970 ± 400	1210 ± 410
$f_{\text{NV}} = 2.87 \text{ GHz}$		
Water	3460 ± 630	930 ± 190
NaCl 500 mM	4830 ± 740	1830 ± 510

Supplementary Note 3: NV-Relaxometry Experiments with Different Organic Solvents

Following measurements are performed in order to investigate the impact of the solvent's physical properties on NV-relaxometry experiments. Therefore, we choose organic solvents with dielectric constants (κ) which differ significantly from the properties of water.⁴⁰ The diamond is covered three times alternatingly with water and the organic solvent. T_1 times of the solvents are then normalized to the T_1 time of water. Figure S3 shows that the T_1 time remains unaffected by the solvent.

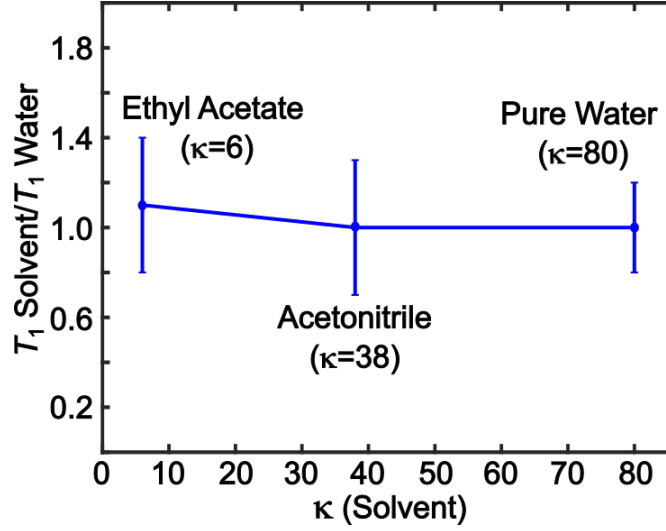


Figure S3: NV-relaxometry experiments showing the impact of the solvent's dielectric constant (κ). Experiments are performed at $f_{\text{NV}} = 1.88$ GHz.

Supplementary Note 4: NV-Relaxometry Measurement Series of Para- and Diamagnetic Electrolyte Solutions in Increasing Concentrations

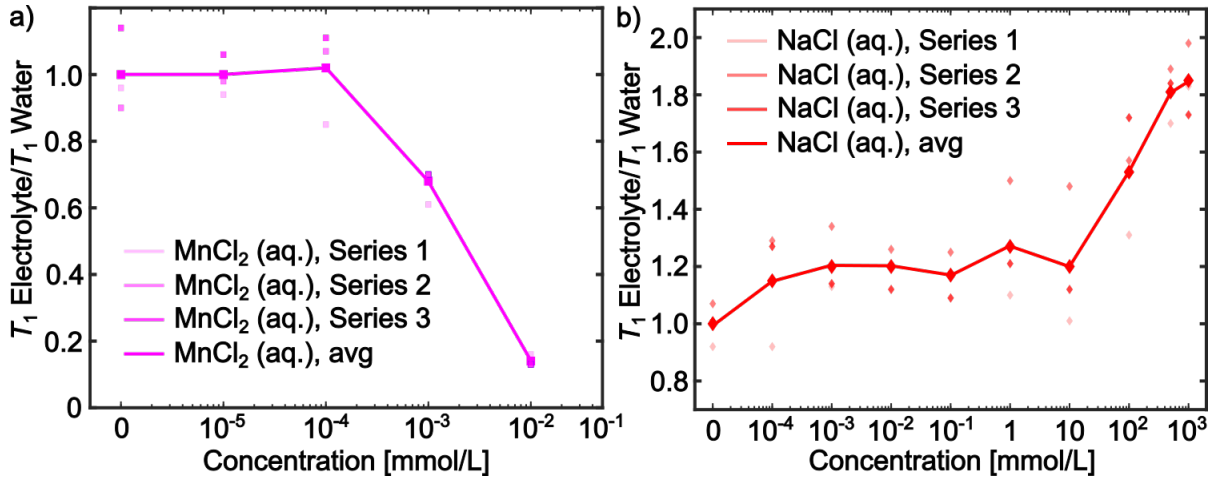


Figure S4: NV-relaxometry measurement series with increasing concentrations of a) MnCl_2 and b) NaCl solutions. Data points are T_1 times normalized to the T_1 time of water for each series. Solid lines connect the mean values of three consecutive performed series. Experiments are performed at $f_{\text{NV}} = 1.88$ GHz.

The NV-relaxometry measurement series with paramagnetic MnCl_2 and diamagnetic NaCl solutions are performed in order to determine the sensitivity of the protocol to increas-

ing electrolyte solutions in each case. Experiments are conducted using the SQ relaxometry pulse sequence (see Methods for detail). We perform each series three times resulting in a mean value for each concentration (see color codes in Figure S4). Figure 2 in the main text shows the mean (normalized) T_1 time along with the standard deviation.

Paramagnetic MnCl_2 solutions decrease the T_1 time in \sim nano- to micromolar concentrations with respect to water. In contrast to that, diamagnetic NaCl solutions increase the T_1 time in \sim millimolar concentrations.

Supplementary Note 5: NV-Depth Dependence Measurements with Water/LiCl (500 mM)

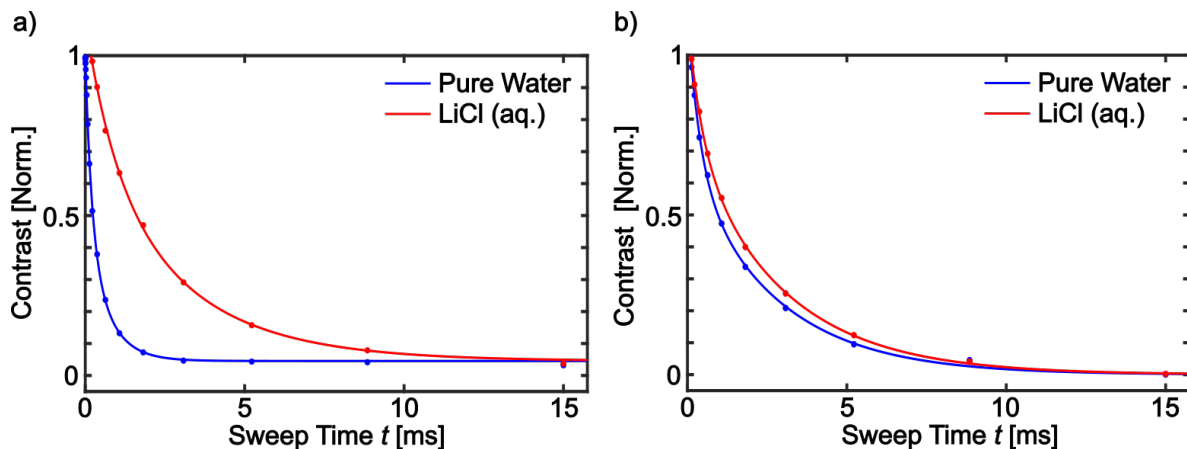


Figure S5: T_1 relaxation curves of water and LiCl 500 mM solution covering the diamond surface. Diamonds were implanted with ^{15}N at an energy of a) 2.5 keV and b) 4 keV. Experiments are performed at $f_{\text{NV}} = 1.88$ GHz.

NV-relaxometry with water/LiCl (500 mM) covering the diamond is performed in order to investigate the impact of another diamagnetic electrolyte and to support the experiments with NaCl (500 mM) solution using differently deep NV-center ensembles (implanted with 2.5 keV and 4 keV, see Figure 3b). Figure S5 and Table S3 show similar results for both NaCl and LiCl (500 mM) solution.

Table S3: T_1 time constants (T_{1a} and T_{1b}) of water, NaCl (500 mM) and LiCl (500 mM) solution on the diamond surface depending on the nitrogen implantation energy. Experiments are performed at $f_{\text{NV}} = 1.88$ GHz.

Implantation energy [keV]		T_{1a} [μs]	T_{1b} [μs]
2.5	Water	940 ± 180	130 ± 20.0
	NaCl 500 mM	1920 ± 200	170 ± 20.0
	Water	660 ± 180	200 ± 50.0
	LiCl 500 mM	2940 ± 720	930 ± 40.0
4	Water	1090 ± 190	190 ± 30.0
	NaCl 500 mM	1270 ± 180	220 ± 40.0
	Water	2750 ± 340	380 ± 80.0
	LiCl 500 mM	2880 ± 270	440 ± 90.0

Supplementary Note 6: NV-Charge State, Coherence and Dephasing Measurements

We observe an increase of T_1 by diamagnetic electrolyte solutions. However, it is known that NV-charge state alteration (i.e., $\text{NV}^0 \leftrightarrow \text{NV}^-$) can influence the outcome of NV-relaxometry measurements.^{67,68} For that reason, we perform NV-Rabi experiments with water/NaCl (500 mM) solution (see Figure S6a). Any change in the NV-Rabi contrast indicates an alteration of the NV-center's charge state. For instance, an ionization of NV^- would increase the proportion of NV^0 , thereby raising the background fluorescence and lowering the contrast. The NV-Rabi experiments show no difference in the outcome between water and the electrolyte implying a constant charge state distribution during the measurement. Secondly, to supplement the NV-Rabi experiments, we conduct NV-relaxometry with distinct optical readout of the NV^0 and NV^- charge states and with three different laser powers (see Figure S6b and Figure S6c). Possible ionization of NV^- in the dark or recombination processes would be visible as an alteration in the readout signal of the NV^0 charge state (see Figure S6b).^{67,68} These measurements are carried out using the first half of the relaxometry pulse sequence (i.e., without a π -pulse) and with two different optical filters. The 647 nm long pass filter predominantly reads out the fluorescence from the NV^- state and the 600 ± 40 nm band pass filter mostly reads out the fluorescence from the NV^0 state.⁶⁹ While a T_1

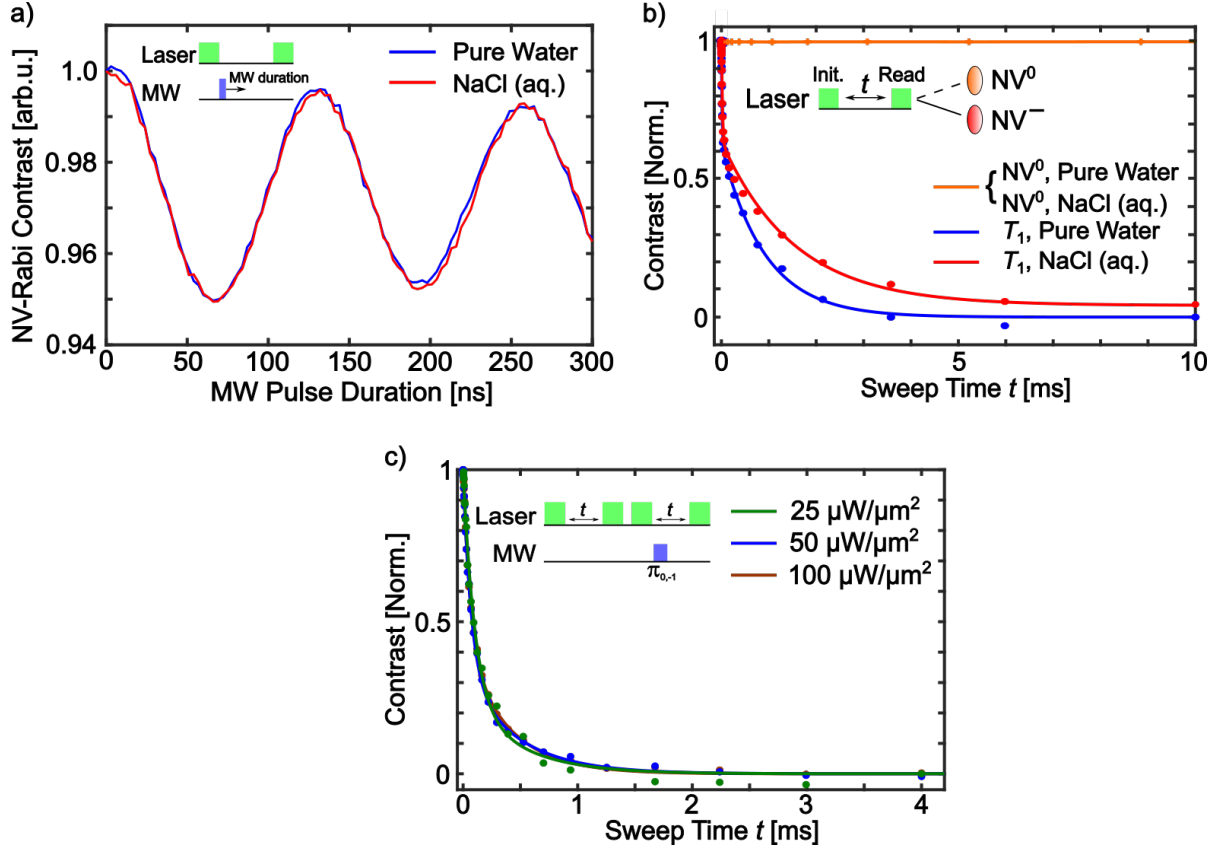


Figure S6: Pulse sequences and spectra of NV-charge state measurements. a) NV-Rabi experiments, b) NV-charge state measurements with selective read-out of the NV^0 or the NV^- state and c) T_1 relaxation curves using three different laser powers.

fluorescence decay curve can be extracted from the measurements with the long pass filter, no decisive change in the NV^0 state is visible using the band pass filter. Probable impact of the laser power on the NV^-/NV^0 ratio and a subsequent change in the T_1 relaxation curves is probed with relaxometry experiments using laser powers of 25, 50 and 100 $\mu\text{W } \mu\text{m}^{-2}$ (see Figure S6c). Both NV-Rabi and NV-charge state experiments do not show an impact on NV-charge state alteration on the relevant timescales of the relaxometry measurements we conduct herein.

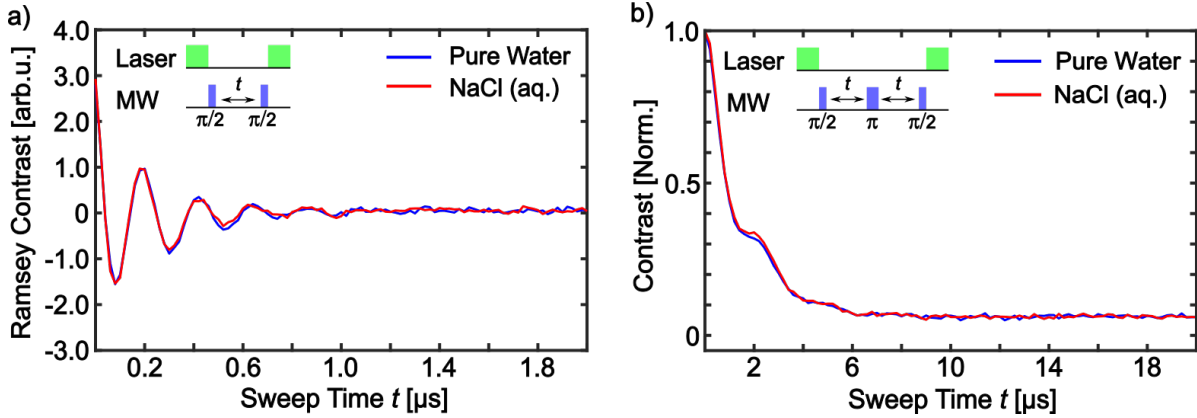


Figure S7: **Pulse sequences and spectra of Ramsey and T_2 Hahn-echo measurements.** a) Ramsey oscillations performed at a 4 MHz detuned $\text{NV}_{0,-1}$ resonance frequency f_{NV} and b) T_2 Hahn-echo experiments with water and NaCl (500 mM) solution covering the diamond surface at $f_{\text{NV}} = 1.88 \text{ GHz}$.

Additionally, we perform Ramsey (NV-dephasing) and T_2 (NV-coherence) Hahn-echo experiments, whose outcome is typically affected by changes in the low frequency components of the noise (see Figure S7a and S7b).³⁰ Both experiments show no difference in the outcome for water or NaCl (500 mM) solution. However, we note that probable changes in this noise frequency regime might not be observable with the high-dense NV-center ensemble we use in this work, since the surrounding spin-bath (e.g. P1-centers or other paramagnetic impurities) is limiting the NV-dephasing and NV-coherence in this case.^{37,50}

Supplementary Note 7: T_1 Time Constants for Single Quantum and Double Quantum Experiments at $B_0 = 15$ G and Zero Field ESR Measurements

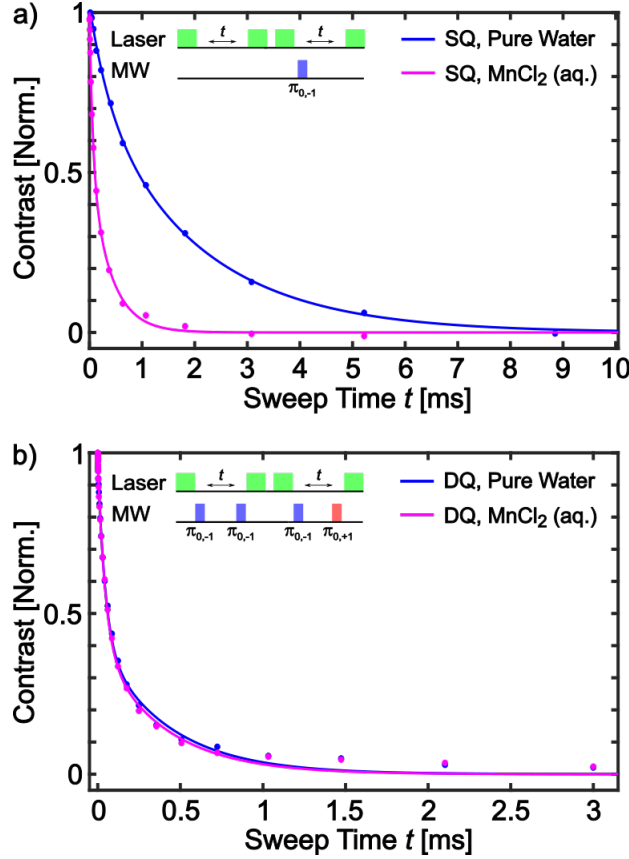


Figure S8: a) SQ and b) DQ relaxation curves of water and MnCl₂ (100 μ M) solution covering the diamond. Experiments are performed at $B_0 = 15$ G, where the NV_{0,-1} transition is at $f_{\text{NV}} = 2.83$ GHz (corresponding to a DQ transition frequency of 80 MHz). $T_{1,\text{SQ}}$ decreases by 80%, whereas $T_{1,\text{DQ}}$ remains unchanged compared to water when MnCl₂ solution covers the diamond.

Single and double quantum T_1 experiments of water/NaCl (500 mM) and water/MnCl₂ (100 μ M) solution covering the diamond surface are performed in order to elucidate the effect of the electrolyte on magnetic and electric field noise. In the case of the NaCl solution, both T_1 time constants ($T_{1a,\text{SQ}}$ and $T_{1a,\text{DQ}}$) increase compared to water, indicating a reduction of both magnetic and electric field noise (see also Table S4). Importantly, MnCl₂ only reduces the T_1 time for the SQ relaxation, whereas the DQ transition remains unaffected compared to

Table S4: T_1 time constants ($T_{1a,SQ}$ and $T_{1a,DQ}$) for water/NaCl (500 mM) and water/MnCl₂ (100 μ M) solution covering the diamond surface. Experiments are performed at $B_0 = 15$ G

	$T_{1a,SQ}$ [μ s]	$T_{1a,DQ}$ [μ s]
Water	2600 ± 280	440 ± 24.0
NaCl 500 mM	3970 ± 400	1250 ± 120
Water	2000 ± 340	410 ± 71
MnCl ₂ 100 μ M	390 ± 71.0	390 ± 78.0

water (see also Table S4). This indicates an exclusive impact of the paramagnetic electrolyte on magnetic field noise. However, we note that probing MnCl₂ in higher (> 100 μ M) concentrations would lead to a collapse of the NV-center's T_1 time (see also Figure 2). Therefore, a final statement on the impact of higher concentrated paramagnetic electrolyte solutions on the DQ (as well as the SQ) relaxation cannot be made.

Additionally, we investigate the static electric field environment of the NV-center, i.e., charges within the diamond and adjacent to the NV-center (e.g., N^+ and NV^-).⁷⁰ Therefore, we measure ESR at zero magnetic field (here the earth's magnetic field ~ 0.5 G), because any difference in the static electric field in the proximity of the NV-center with respect to water or the electrolyte solution covering the surface would induce a shifting and/or splitting of the $m_s = \pm 1$ states apparent in the ESR spectra.⁷⁰ Figure S9 shows no significant change of the ESR resonance lines for the exposure of water or electrolyte solution, indicating that static electric fields do not contribute.

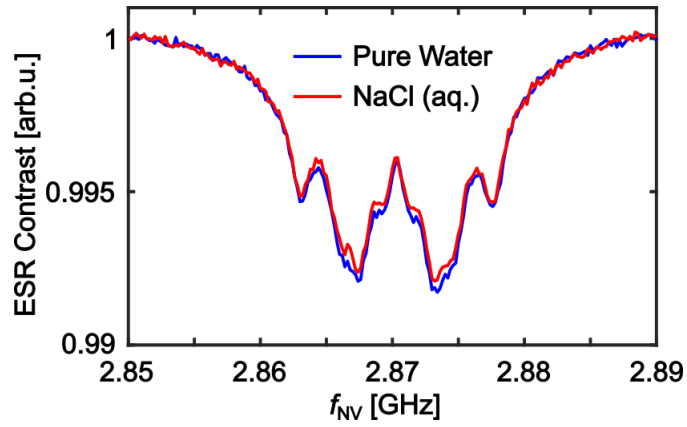


Figure S9: ESR experiments at zero magnetic field with water and NaCl (500 mM) solution covering the diamond surface.

Supplementary Note 8: Results of DFT-PBE *Ab Initio* Molecular Dynamics Simulations

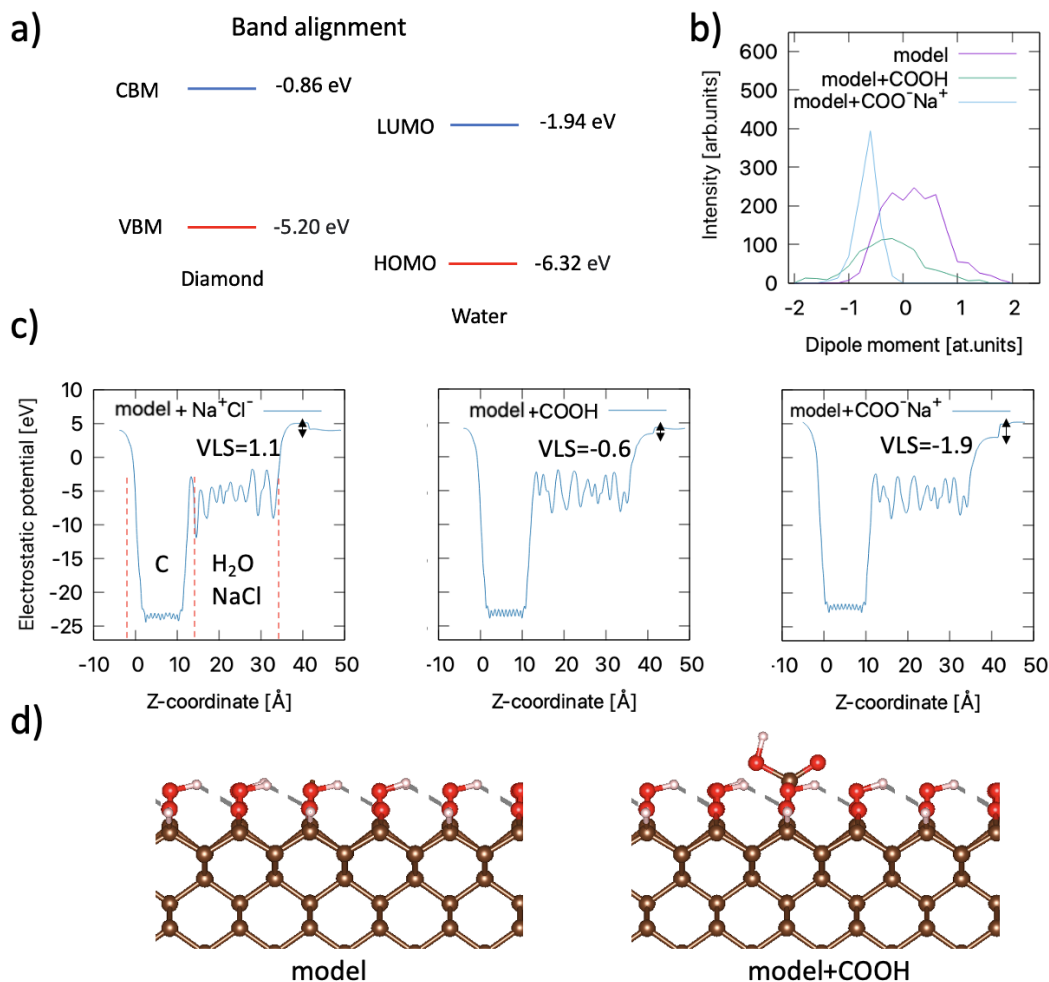


Figure S10: a) Band alignment of the water layer and the model diamond surface. b) Distribution of interfacial dipoles, sampled from the MD trajectories for three different compositions of the interface and solvent. c) Average electrostatic potentials and vacuum level shifts (VLS) computed for the configurations corresponding to the middle of the distributions in b). Vertical lines show the parts of the simulation box, spanned by diamond (C), water or aqueous NaCl solution and vacuum. d) Structures of the model diamond surface before and after adding a COOH group.

References

- (1) Acosta, V. M.; Bauch, E.; Ledbetter, M. P.; Waxman, A.; Bouchard, L.-S.; Budker, D. Temperature Dependence of the Nitrogen-Vacancy Magnetic Resonance in Diamond. *Physical Review Letters* **2010**, *104*, 070801.
- (2) Ivády, V.; Simon, T.; Maze, J. R.; Abrikosov, I. A.; Gali, A. Pressure and temperature dependence of the zero-field splitting in the ground state of NV centers in diamond: A first-principles study. *Physical Review B* **2014**, *90*, 235205.
- (3) Teissier, J.; Barfuss, A.; Appel, P.; Neu, E.; Maletinsky, P. Strain Coupling of a Nitrogen-Vacancy Center Spin to a Diamond Mechanical Oscillator. *Physical Review Letters* **2014**, *113*, 020503.
- (4) Dolde, F.; Fedder, H.; Doherty, M. W.; Nöbauer, T.; Rempp, F.; Balasubramanian, G.; Wolf, T.; Reinhard, F.; Hollenberg, L. C. L.; Jelezko, F.; Wrachtrup, J. Electric-field sensing using single diamond spins. *Nature Physics* **2011**, *7*, 459–463.
- (5) Balasubramanian, G.; Chan, I. Y.; Kolesov, R.; Al-Hmoud, M.; Tisler, J.; Shin, C.; Kim, C.; Wojcik, A.; Hemmer, P. R.; Krueger, A.; Hanke, T.; Leitenstorfer, A.; Bratschkitsch, R.; Jelezko, F.; Wrachtrup, J. Nanoscale imaging magnetometry with diamond spins under ambient conditions. *Nature* **2008**, *455*, 648–651.
- (6) Maze, J. R.; Stanwix, P. L.; Hodges, J. S.; Hong, S.; Taylor, J. M.; Cappellaro, P.; Jiang, L.; Dutt, M. V. G.; Togan, E.; Zibrov, A. S.; Yacoby, A.; Walsworth, R. L.; Lukin, M. D. Nanoscale magnetic sensing with an individual electronic spin in diamond. *Nature* **2008**, *455*, 644–647.
- (7) Glenn, D. R.; Lee, K.; Park, H.; Weissleder, R.; Yacoby, A.; Lukin, M. D.; Lee, H.; Walsworth, R. L.; Connolly, C. B. Single-cell magnetic imaging using a quantum diamond microscope. *Nature Methods* **2015**, *12*, 736–738.

- (8) Lovchinsky, I.; Sushkov, A. O.; Urbach, E.; de Leon, N. P.; Choi, S.; De Greve, K.; Evans, R.; Gertner, R.; Bersin, E.; Muller, C.; McGuinness, L.; Jelezko, F.; Walsworth, R. L.; Park, H.; Lukin, M. D. Nuclear magnetic resonance detection and spectroscopy of single proteins using quantum logic. *Science* **2016**, *351*, 836–841.
- (9) Müller, C.; Kong, X.; Cai, J.-M.; Melentijević, K.; Stacey, A.; Markham, M.; Twitchen, D.; Isoya, J.; Pezzagna, S.; Meijer, J.; Du, J. F.; Plenio, M. B.; Naydenov, B.; McGuinness, L. P.; Jelezko, F. Nuclear magnetic resonance spectroscopy with single spin sensitivity. *Nature Communications* **2014**, *5*, 4703.
- (10) Sushkov, A. O.; Lovchinsky, I.; Chisholm, N.; Walsworth, R. L.; Park, H.; Lukin, M. D. Magnetic Resonance Detection of Individual Proton Spins Using Quantum Reporters. *Physical Review Letters* **2014**, *113*, 197601.
- (11) Bucher, D. B. Principles of nano-and microscale NMR-spectroscopy with NV-diamond sensors. *eMagRes* **2019**, *8*, 363–370.
- (12) Lovchinsky, I.; Sanchez-Yamagishi, J. D.; Urbach, E. K.; Choi, S.; Fang, S.; Andersen, T. I.; Watanabe, K.; Taniguchi, T.; Bylinskii, A.; Kaxiras, E.; Kim, P.; Park, H.; Lukin, M. D. Magnetic resonance spectroscopy of an atomically thin material using a single-spin qubit. *Science* **2017**, *355*, 503–507.
- (13) Liu, K. S.; Henning, A.; Heindl, M. W.; Allert, R. D.; Bartl, J. D.; Sharp, I. D.; Rizzato, R.; Bucher, D. B. Surface NMR using quantum sensors in diamond. *Proceedings of the National Academy of Sciences* **2022**, *119*, e2111607119.
- (14) Allert, R. D.; Briegel, K. D.; Bucher, D. B. Advances in nano- and microscale NMR spectroscopy using diamond quantum sensors. *Chemical Communications* **2022**, *58*, 8165–8181.
- (15) Allert, R. D.; Bruckmaier, F.; Neuling, N. R.; Freire-Moschovitis, F. A.; Liu, K. S.;

- Schrepel, C.; Schätzle, P.; Knittel, P.; Hermans, M.; Bucher, D. B. Microfluidic quantum sensing platform for lab-on-a-chip applications. *Lab on a Chip* **2022**, *22*, 4831–4840.
- (16) Shi, F.; Zhang, Q.; Wang, P.; Sun, H.; Wang, J.; Rong, X.; Chen, M.; Ju, C.; Reinhard, F.; Chen, H.; Wrachtrup, J.; Wang, J.; Du, J. Single-protein spin resonance spectroscopy under ambient conditions. *Science* **2015**, *347*, 1135–1138.
- (17) Schirhagl, R.; Chang, K.; Loretz, M.; Degen, C. L. Nitrogen-Vacancy Centers in Diamond: Nanoscale Sensors for Physics and Biology. *Annual Review of Physical Chemistry* **2014**, *65*, 83–105.
- (18) Bucher, D. B.; Aude Craik, D. P.; Backlund, M. P.; Turner, M. J.; Ben Dor, O.; Glenn, D. R.; Walsworth, R. L. Quantum diamond spectrometer for nanoscale NMR and ESR spectroscopy. *Nature Protocols* **2019**, *14*, 2707–2747.
- (19) Kim, M.; Mamin, H. J.; Sherwood, M. H.; Ohno, K.; Awschalom, D. D.; Rugar, D. Decoherence of Near-Surface Nitrogen-Vacancy Centers Due to Electric Field Noise. *Physical Review Letters* **2015**, *115*, 087602.
- (20) Stacey, A.; Dontschuk, N.; Chou, J.; Broadway, D. A.; Schenk, A. K.; Sear, M. J.; Tetienne, J.; Hoffman, A.; Prawer, S.; Pakes, C. I.; Tadich, A.; de Leon, N. P.; Gali, A.; Hollenberg, L. C. L. Evidence for Primal sp^2 Defects at the Diamond Surface: Candidates for Electron Trapping and Noise Sources. *Advanced Materials Interfaces* **2019**, *6*, 1801449.
- (21) Sangtawesin, S. et al. Origins of Diamond Surface Noise Probed by Correlating Single-Spin Measurements with Surface Spectroscopy. *Physical Review X* **2019**, *9*, 031052.
- (22) Romach, Y.; Müller, C.; Unden, T.; Rogers, L. J.; Isoda, T.; Itoh, K. M.; Markham, M.; Stacey, A.; Meijer, J.; Pezzagna, S.; Naydenov, B.; McGuinness, L. P.; Bar-Gill, N.; Jelezko, F. Spectroscopy of Surface-Induced Noise Using Shallow Spins in Diamond. *Physical Review Letters* **2015**, *114*, 017601.

- (23) Chrostoski, P.; Sadeghpour, H. R.; Santamore, D. H. Electric Noise Spectra of a Near-Surface Nitrogen-Vacancy Center in Diamond with a Protective Layer. *Physical Review Applied* **2018**, *10*, 064056.
- (24) Degen, C. L.; Reinhard, F.; Cappellaro, P. Quantum sensing. *Reviews of Modern Physics* **2017**, *89*, 035002.
- (25) Steinert, S.; Ziem, F.; Hall, L. T.; Zappe, A.; Schweikert, M.; Götz, N.; Aird, A.; Balasubramanian, G.; Hollenberg, L.; Wrachtrup, J. Magnetic spin imaging under ambient conditions with sub-cellular resolution. *Nature Communications* **2013**, *4*, 1607.
- (26) Mzyk, A.; Sigaeva, A.; Schirhagl, R. Relaxometry with Nitrogen Vacancy (NV) Centers in Diamond. *Accounts of Chemical Research* **2022**, *55*, 3572–3580.
- (27) Perona Martínez, F.; Nusantara, A. C.; Chipaux, M.; Padamati, S. K.; Schirhagl, R. Nanodiamond Relaxometry-Based Detection of Free-Radical Species When Produced in Chemical Reactions in Biologically Relevant Conditions. *ACS Sensors* **2020**, *5*, 3862–3869.
- (28) Li, R.; Vedelaar, T.; Mzyk, A.; Morita, A.; Padamati, S. K.; Schirhagl, R. Following Polymer Degradation with Nanodiamond Magnetometry. *ACS Sensors* **2022**, *7*, 123–130.
- (29) Jarmola, A.; Acosta, V. M.; Jensen, K.; Chemerisov, S.; Budker, D. Temperature- and Magnetic-Field-Dependent Longitudinal Spin Relaxation in Nitrogen-Vacancy Ensembles in Diamond. *Physical Review Letters* **2012**, *108*, 197601.
- (30) Rosskopf, T.; Dussaux, A.; Ohashi, K.; Loretz, M.; Schirhagl, R.; Watanabe, H.; Shikata, S.; Itoh, K. M.; Degen, C. L. Investigation of Surface Magnetic Noise by Shallow Spins in Diamond. *Physical Review Letters* **2014**, *112*, 147602.

- (31) Nie, L.; Nusantara, A. C.; Damle, V. G.; Baranov, M. V.; Chipaux, M.; Reyes-San-Martin, C.; Hamoh, T.; Epperla, C. P.; Guricova, M.; Cigler, P.; van den Bogaart, G.; Schirhagl, R. Quantum Sensing of Free Radicals in Primary Human Dendritic Cells. *Nano Letters* **2022**, *22*, 1818–1825.
- (32) Ziem, F. C.; Götz, N. S.; Zappe, A.; Steinert, S.; Wrachtrup, J. Highly Sensitive Detection of Physiological Spins in a Microfluidic Device. *Nano Letters* **2013**, *13*, 4093–4098.
- (33) Ermakova, A.; Pramanik, G.; Cai, J.-M.; Algara-Siller, G.; Kaiser, U.; Weil, T.; Tzeng, Y.-K.; Chang, H. C.; McGuinness, L. P.; Plenio, M. B.; Naydenov, B.; Jelezko, F. Detection of a Few Metallo-Protein Molecules Using Color Centers in Nanodiamonds. *Nano Letters* **2013**, *13*, 3305–3309.
- (34) Fujisaku, T.; Tanabe, R.; Onoda, S.; Kubota, R.; Segawa, T. F.; So, F. T.-K.; Ohshima, T.; Hamachi, I.; Shirakawa, M.; Igarashi, R. pH Nanosensor Using Electronic Spins in Diamond. *ACS Nano* **2019**, *13*, 11726–11732.
- (35) Simpson, D. A.; Ryan, R. G.; Hall, L. T.; Panchenko, E.; Drew, S. C.; Petrou, S.; Donnelly, P. S.; Mulvaney, P.; Hollenberg, L. C. L. Electron paramagnetic resonance microscopy using spins in diamond under ambient conditions. *Nature Communications* **2017**, *8*, 458.
- (36) Pham, L. M.; DeVience, S. J.; Casola, F.; Lovchinsky, I.; Sushkov, A. O.; Bersin, E.; Lee, J.; Urbach, E.; Cappellaro, P.; Park, H.; Yacoby, A.; Lukin, M.; Walsworth, R. L. NMR technique for determining the depth of shallow nitrogen-vacancy centers in diamond. *Physical Review B* **2016**, *93*, 045425.
- (37) Henshaw, J.; Kehayias, P.; Saleh Ziabari, M.; Titze, M.; Morissette, E.; Watanabe, K.; Taniguchi, T.; Li, J. I. A.; Acosta, V. M.; Bielejec, E. S.; Lilly, M. P.; Mounce, A. M. Nanoscale solid-state nuclear quadrupole resonance spectroscopy using depth-optimized nitrogen-vacancy ensembles in diamond. *Applied Physics Letters* **2022**, *120*, 174002.

- (38) Brown, K. J.; Chartier, E.; Sweet, E. M.; Hopper, D. A.; Bassett, L. C. Cleaning diamond surfaces using boiling acid treatment in a standard laboratory chemical hood. *Journal of Chemical Health & Safety* **2019**, *26*, 40–44.
- (39) Li, C.; Zhang, X.; Oliveira, E. F.; Puthirath, A. B.; Neupane, M. R.; Weil, J. D.; Birdwell, A. G.; Ivanov, T. G.; Kong, S.; Gray, T.; Kannan, H.; Biswas, A.; Vajtai, R.; Galvao, D. S.; Ajayan, P. M. Systematic comparison of various oxidation treatments on diamond surface. *Carbon* **2021**, *182*, 725–734.
- (40) Seyferth, D. Organic Solvents. Physical Properties and Methods of Purification. Fourth Edition. Volume 11 of Weissberger's "Techniques of Chemistry". *Organometallics* **1987**, *6*, 1375–1376.
- (41) Flora, S. J. *Biomarkers in Toxicology*; Elsevier, 2014; pp 485–519.
- (42) Flowers, T. J.; Munns, R.; Colmer, T. D. Sodium chloride toxicity and the cellular basis of salt tolerance in halophytes. *Annals of Botany* **2015**, *115*, 419–431.
- (43) Ladenson, J. H.; Apple, F. S.; Aguanno, J. J.; Koch, D. D. Sodium measurements in multiple myeloma: two techniques compared. *Clinical Chemistry* **1982**, *28*, 2383–2386.
- (44) Bard, A. J.; Faulkner, L. R. *Electrochemical Methods: Fundamentals and Applications*, 2nd ed.; Wiley, 2001.
- (45) Myers, B. A.; Ariyaratne, A.; Jayich, A. C. B. Double-Quantum Spin-Relaxation Limits to Coherence of Near-Surface Nitrogen-Vacancy Centers. *Physical Review Letters* **2017**, *118*, 197201.
- (46) Sushkov, A. O.; Lovchinsky, I.; Chisholm, N.; Walsworth, R. L.; Park, H.; Lukin, M. D. Magnetic Resonance Detection of Individual Proton Spins Using Quantum Reporters. *Physical Review Letters* **2014**, *113*, 197601.

- (47) Schlipf, L.; Oeckinghaus, T.; Xu, K.; Dasari, D. B. R.; Zappe, A.; de Oliveira, F. F.; Kern, B.; Azarkh, M.; Drescher, M.; Ternes, M.; Kern, K.; Wrachtrup, J.; Finkler, A. A molecular quantum spin network controlled by a single qubit. *Science Advances* **2017**, *3*.
- (48) Mamin, H. J.; Sherwood, M. H.; Rugar, D. Detecting external electron spins using nitrogen-vacancy centers. *Physical Review B* **2012**, *86*, 195422.
- (49) Bluvstein, D.; Zhang, Z.; McLellan, C. A.; Williams, N. R.; Jayich, A. C. B. Extending the Quantum Coherence of a Near-Surface Qubit by Coherently Driving the Paramagnetic Surface Environment. *Physical Review Letters* **2019**, *123*, 146804.
- (50) Barry, J. F.; Schloss, J. M.; Bauch, E.; Turner, M. J.; Hart, C. A.; Pham, L. M.; Walsworth, R. L. Sensitivity optimization for NV-diamond magnetometry. *Reviews of Modern Physics* **2020**, *92*, 015004.
- (51) Zhang, Z.; Joos, M.; Bluvstein, D.; Lyu, Y.; Jayich, A. C. B. Reporter-spin-assisted T1 relaxometry. **2022**, arXiv:2208.11470 [quant-ph].
- (52) Fávaro de Oliveira, F.; Antonov, D.; Wang, Y.; Neumann, P.; Momenzadeh, S. A.; Häußermann, T.; Pasquarelli, A.; Denisenko, A.; Wrachtrup, J. Tailoring spin defects in diamond by lattice charging. *Nature Communications* **2017**, *8*, 15409.
- (53) Sies, H.; Jones, D. P. Reactive oxygen species (ROS) as pleiotropic physiological signalling agents. *Nature Reviews Molecular Cell Biology* **2020**, *21*, 363–383.
- (54) Favaro, M.; Jeong, B.; Ross, P. N.; Yano, J.; Hussain, Z.; Liu, Z.; Crumlin, E. J. Unravelling the electrochemical double layer by direct probing of the solid/liquid interface. *Nature Communications* **2016**, *7*, 12695.
- (55) Kaufmann, S.; Simpson, D. A.; Hall, L. T.; Perunicic, V.; Senn, P.; Steinert, S.; McGuinness, L. P.; Johnson, B. C.; Ohshima, T.; Caruso, F.; Wrachtrup, J.

- Scholten, R. E.; Mulvaney, P.; Hollenberg, L. Detection of atomic spin labels in a lipid bilayer using a single-spin nanodiamond probe. *Proceedings of the National Academy of Sciences* **2013**, *110*, 10894–10898.
- (56) Hall, L. T.; Hill, C. D.; Cole, J. H.; Städler, B.; Caruso, F.; Mulvaney, P.; Wrachtrup, J.; Hollenberg, L. C. L. Monitoring ion-channel function in real time through quantum decoherence. *Proceedings of the National Academy of Sciences* **2010**, *107*, 18777–18782.
- (57) Szatmári, D.; Sárkány, P.; Kocsis, B.; Nagy, T.; Miseta, A.; Barkó, S.; Longauer, B.; Robinson, R. C.; Nyitrai, M. Intracellular ion concentrations and cation-dependent remodelling of bacterial MreB assemblies. *Scientific Reports* **2020**, *10*, 12002.
- (58) Henning, A.; Bartl, J. D.; Zeidler, A.; Qian, S.; Bienek, O.; Jiang, C.; Paulus, C.; Rieger, B.; Stutzmann, M.; Sharp, I. D. Aluminum Oxide at the Monolayer Limit via Oxidant-Free Plasma-Assisted Atomic Layer Deposition on GaN. *Advanced Functional Materials* **2021**, *31*, 2101441.
- (59) Kaviani, M.; Deák, P.; Aradi, B.; Frauenheim, T.; Chou, J.-P.; Gali, A. Proper Surface Termination for Luminescent Near-Surface NV Centers in Diamond. *Nano Letters* **2014**, *14*, 4772–4777.
- (60) Berendsen, H.; van der Spoel, D.; van Drunen, R. GROMACS: A message-passing parallel molecular dynamics implementation. *Computer Physics Communications* **1995**, *91*, 43–56.
- (61) Schmid, N.; Eichenberger, A. P.; Choutko, A.; Riniker, S.; Winger, M.; Mark, A. E.; van Gunsteren, W. F. Definition and testing of the GROMOS force-field versions 54A7 and 54B7. *European Biophysics Journal* **2011**, *40*, 843–856.
- (62) Kresse, G.; Furthmüller, J. Efficient iterative schemes for ab initio total-energy calculations using a plane-wave basis set. *Physical Review B* **1996**, *54*, 11169–11186.

- (63) Perdew, J. P.; Burke, K.; Ernzerhof, M. Generalized Gradient Approximation Made Simple. *Physical Review Letters* **1996**, *77*, 3865–3868.
- (64) Marcus, R. A. On the Theory of Oxidation-Reduction Reactions Involving Electron Transfer. I. *The Journal of Chemical Physics* **1956**, *24*, 966–978.
- (65) Broadway, D. A.; Dontschuk, N.; Tsai, A.; Lillie, S. E.; Lew, C. T.-K.; McCallum, J. C.; Johnson, B. C.; Doherty, M. W.; Stacey, A.; Hollenberg, L. C. L.; Tetienne, J.-P. Spatial mapping of band bending in semiconductor devices using in situ quantum sensors. *Nature Electronics* **2018**, *1*, 502–507.
- (66) Rioux, J. A.; Levesque, I. R.; Rutt, B. K. Biexponential longitudinal relaxation in white matter: Characterization and impact on T1 mapping with IR-FSE and MP2RAGE. *Magnetic Resonance in Medicine* **2016**, *75*, 2265–2277.
- (67) Bluvstein, D.; Zhang, Z.; Jayich, A. C. B. Identifying and Mitigating Charge Instabilities in Shallow Diamond Nitrogen-Vacancy Centers. *Physical Review Letters* **2019**, *122*, 076101.
- (68) Dhomkar, S.; Jayakumar, H.; Zangara, P. R.; Meriles, C. A. Charge Dynamics in near-Surface, Variable-Density Ensembles of Nitrogen-Vacancy Centers in Diamond. *Nano Letters* **2018**, *18*, 4046–4052.
- (69) Doherty, M. W.; Manson, N. B.; Delaney, P.; Jelezko, F.; Wrachtrup, J.; Hollenberg, L. C. The nitrogen-vacancy colour centre in diamond. *Physics Reports* **2013**, *528*, 1–45.
- (70) Mittiga, T.; Hsieh, S.; Zu, C.; Kobrin, B.; Machado, F.; Bhattacharyya, P.; Rui, N. Z.; Jarmola, A.; Choi, S.; Budker, D.; Yao, N. Y. Imaging the Local Charge Environment of Nitrogen-Vacancy Centers in Diamond. *Physical Review Letters* **2018**, *121*, 246402.